JGR Oceans

RESEARCH ARTICLE
10.1029/2021JC018304

Comparison of Nitrate Isotopes Between the South China Sea and Western North Pacific Ocean: Insights Into Biogeochemical Signals and Water Exchange

Jin-Yu Terence Yang[1], Jin-Ming Tang[1], Sijing Kang[1], Minhan Dai[1], Shuh-Ji Kao[1,2], Xiuli Yan[3], Min Nina Xu[2], and Chuanjun Du[2]

[1]State Key Laboratory of Marine Environmental Science, College of Ocean and Earth Sciences, Xiamen University, Xiamen, China, [2]State Key Laboratory of Marine Resource Utilization in South China Sea, Hainan University, Haikou, China, [3]Institute of Marine Science and Guangdong Provincial Key Laboratory of Marine Biotechnology, College of Science, Shantou University, Shantou, China

Abstract Reconstructing past changes in the oceanic nitrate inventory with sedimentary N records in the South China Sea (SCS), which is the terminal of North Pacific Intermediate Water (NPIW), has regional and global implications. However, water-column nitrate cycling that affects N isotope preservation remains poorly understood in the SCS. We present a new data set of nitrate isotopes ($\delta^{15}N_{NO_3}$ and $\delta^{18}O_{NO_3}$) to elucidate nitrate dynamics in the SCS and the adjoining western North Pacific Ocean (wNPO). Greater increases in $\delta^{18}O_{NO_3}$ than in $\delta^{15}N_{NO_3}$ are observed in the SCS euphotic zone, suggesting a combined effect of partial nitrate assimilation and nitrification. In the subsurface and thermocline waters of both regions, upward disproportional decreases in $\delta^{15}N_{NO_3}$ and $\delta^{18}O_{NO_3}$ accompanied by elevated nitrate anomalies (N*) indicate an accumulation of external N. Such changes are less significant in the SCS due to higher nitrate concentrations therein, although external N influxes are comparable in both regions. High $\delta^{15}N_{NO_3}$ and $\delta^{18}O_{NO_3}$ values in the wNPO intermediate water result from the lateral transport of NPIW with isotopically more enriched nitrate from the remote denitrification zones followed by mixing with overlying water containing isotopically depleted nitrate. As NPIW flows into the SCS, its isotopically enriched signal is further diluted by strong vertical mixing with overlying and underlying waters in the interior. Compared to its source water from the wNPO, the SCS deep water has consistent nitrate isotopic compositions but significantly lower N*, indicating increased benthic denitrification at the wNPO margins with an estimated rate of 0.26–0.41 mmol N m^{-2} day^{-1}.

Plain Language Summary The South China Sea (SCS) is an ideal region to study past changes in the oceanic N pool using sedimentary N records. These records are sensitive to water-column nitrate cycling. This study presents a new data set of nitrate isotopes in the SCS and the neighboring western North Pacific Ocean, the aim of which is to determine major processes controlling their distribution. Partial nitrate consumption by phytoplankton and nitrate production from ammonium/nitrite oxidation by microorganisms together determine nitrate isotopes in the upper 100 m of the SCS. Atmospheric-derived and biologically fixed N that provides lighter nitrate isotopes mainly accumulates in the subsurface water (100–400 m). In deeper waters, the distribution of nitrate isotopes in the SCS is regulated by a vertical sandwich-like water flow structure through the Luzon Strait, that is westward inflows of the North Pacific waters in the upper (<750 m) and deep (>1,500 m) layers and an eastward outflow of SCS waters between the two layers. Strong vertical mixing in the SCS interior further smooths the original nitrate isotopes. Our findings highlight the important role of these biogeochemical and physical processes in governing water-column nitrate isotopes and thus sedimentary N records in the SCS.

Key Points:

- Nitrate $\delta^{15}N$ and $\delta^{18}O$ increase unequally in the South China Sea (SCS) surface water due to partial nitrate assimilation and nitrification
- External N inputs lower $\delta^{15}N$ and $\delta^{18}O$ of subsurface nitrate to a lesser extent in the SCS than in the western North Pacific Ocean (wNPO)
- Lateral exchange between SCS and wNPO intermediate and deep waters along with vertical mixing modifies their nitrate isotopic composition

Supporting Information:

Supporting Information may be found in the online version of this article.

Correspondence to:

J.-Y. T. Yang,
jyyang@xmu.edu.cn

Citation:

Yang, J.-Y. T., Tang, J.-M., Kang, S., Dai, M., Kao, S.-J., Yan, X., et al. (2022). Comparison of nitrate isotopes between the South China Sea and western North Pacific Ocean: Insights into biogeochemical signals and water exchange. *Journal of Geophysical Research: Oceans*, *127*, e2021JC018304. https://doi.org/10.1029/2021JC018304

Received 9 DEC 2021
Accepted 15 APR 2022

Author Contributions:

Conceptualization: Jin-Yu Terence Yang, Minhan Dai, Shuh-Ji Kao
Formal analysis: Jin-Yu Terence Yang, Sijing Kang
Funding acquisition: Jin-Yu Terence Yang, Minhan Dai, Shuh-Ji Kao
Investigation: Jin-Yu Terence Yang, Jin-Ming Tang, Sijing Kang, Xiuli Yan, Min Nina Xu, Chuanjun Du
Methodology: Jin-Yu Terence Yang, Jin-Ming Tang, Sijing Kang, Shuh-Ji Kao, Xiuli Yan, Min Nina Xu, Chuanjun Du
Project Administration: Jin-Yu Terence Yang, Minhan Dai, Shuh-Ji Kao
Resources: Minhan Dai, Shuh-Ji Kao
Software: Sijing Kang
Supervision: Jin-Yu Terence Yang, Minhan Dai, Shuh-Ji Kao

1. Introduction

The nitrogen (N) cycle in marginal seas, as an important component of global marine biogeochemistry and the Earth's climate system, is dynamic and complicated (Gruber & Galloway, 2008; Voss et al., 2013). Marginal seas receive considerable amounts of human-derived N via atmospheric transport and river input (Jickells et al., 2017); on the other hand, waters in the marginal sea communicate with the open ocean, which substantially affects the nutrient distribution, budget and cycling in its interior (Chen, 2010; Dai et al., 2013; Xu et al., 2018). The impacts of anthropogenic activities and communication with the open ocean have been imprinted into nutrient

Validation: Chuanjun Du
Visualization: Jin-Ming Tang
Writing – original draft: Jin-Yu Terence Yang
Writing – review & editing: Jin-Yu Terence Yang

stoichiometry (Kim et al., 2011; Moon et al., 2021) and N isotopic records in the water column and sediments (Emeis et al., 2010; Kienast, 2000; Kim et al., 2017), with important implications for the evolution of marine primary productivity and climate change (Canfield et al., 2010; Doney, 2010).

The South China Sea (SCS) is one of the world's largest marginal seas located in the tropical and subtropical western North Pacific Ocean (wNPO). The SCS surface water is oligotrophic during most of the year, with nitracline depths (defined as the depth with nitrate concentration higher than 0.1 μmol kg^{-1}; Yang et al., 2017) of 50–75 m, which are deeper than the mixed layer depth (Du et al., 2013). The environmental conditions of the SCS, with high temperature, stratification, low nutrient and high iron input in the surface waters, favor the growth of diazotrophs (Wong et al., 2002). However, the average rate of N_2 fixation is 51.7 ± 6.2 μmol N m^{-2} d^{-1} in the SCS, which is significantly lower than that of the Kuroshio Current (KC, 142.7 ± 29.6 μmol N m^{-2} d^{-1}) in the adjacent wNPO (Chen et al., 2014; Shiozaki et al., 2010). Instead, atmospheric N deposition (AND), mainly derived from anthropogenic activities, is an important pathway that introduces external N to the SCS surface, thereby promoting phytoplankton productivity therein (Shi et al., 2021; Yang et al., 2014). The flux of AND to the SCS is approximately 150 μmol N m^{-2} d^{-1}, which is higher than those of N_2 fixation and riverine nitrogen input (Kim et al., 2014). In addition to these external sources of new N, upwelled nitrate from the subsurface primarily supports new production and particle export in the SCS basin (Yang et al., 2017).

Communication of water masses between the SCS and wNPO through the Luzon Strait (LS) with the deepest sill of ~2,200 m, the unique deep water channel at the boundary of the Indo-Pacific Water Pool, is vigorous (Figure 1; Liu & Gan, 2017). A westward intrusion of the KC exists in the upper layer (0–750 m), and it strengthens during wintertime. Approximately 10% of the intrusive KC subducts to the intermediate layer (750–1,500 m) in the SCS basin. On the other hand, the denser wNPO deep water (>1,500 m) inflows westward into the SCS across the LS sill and then subducts in the northern basin; as a result, the deep water overflow into the SCS with a cyclonic circulation induces a basin-scale deep upwelling in the interior and subsequently contributes to the intermediate waters. The subducted waters from the upper layer and the upwelled waters from the deep layer together form an eastward outflow of the SCS intermediate waters through the LS. As such, a vertical sandwich-like water flow structure through the LS has been recognized (Cai et al., 2020). The extensive water exchange suggests a close coupling between nitrate (NO_3^-) reservoirs in the SCS basin and the Pacific Ocean. Changes in the Pacific circulation and regional monsoon intensity may influence the depth/thickness of the SCS thermocline, which could affect N isotopic composition of shallow subsurface NO_3^- and subsequently N records in sinking particles and sediments (Ren et al., 2012; Yang et al., 2017). Sedimentary N isotope records in the SCS basin are thus sensitive to past changes in ocean circulation, the intensity of the East Asian monsoon and the variability in the El Niño-Southern Oscillation, which have been used to reconstruct variations in oceanic nitrate inventory and paleoproductivity on local/regional and even global scales (Higginson et al., 2003; Kienast, 2000; Ren et al., 2012). To comprehensively interpret these sedimentary N archives, it is crucial to better elucidate the water-column NO_3^- cycling in the SCS and its interaction with the wNPO.

N isotopic composition of NO_3^- ($\delta^{15}N_{NO_3} = (({}^{15}N/{}^{14}N_{sample})/({}^{15}N/{}^{14}N_{standard}) - 1) \times 1{,}000‰$, which is referenced to air N_2) has been widely applied to quantify the magnitude of oceanic N input and output (e.g., Knapp et al., 2008; Marconi et al., 2017; Voss et al., 2001). It also documents information on the origin and history of water masses (Marconi et al., 2015; Rafter et al., 2012; Tuerena et al., 2015; Yoshikawa et al., 2015). Moreover, due to different pathways of N and O via nitrate consumption and production, O isotopic composition of NO_3^- ($\delta^{18}O_{NO_3} = (({}^{18}O/{}^{16}O_{sample})/({}^{18}O/{}^{16}O_{standard}) - 1) \times 1{,}000‰$, which is referenced to Vienna Standard Mean Ocean Water (VSMOW)) provides an additional constraint to distinguish multiple overprinting processes (e.g., Sigman et al., 2005). In general, the consumption of seawater NO_3^- (e.g., nitrate assimilation and denitrification) has consistent N and O isotopic effects, leading to parallel increases in $\delta^{15}N_{NO_3}$ and $\delta^{18}O_{NO_3}$ in the residual NO_3^- pool (Granger et al., 2008; Kritee et al., 2012). In this case, the Δ(15–18) values (i.e., the differences between $\delta^{15}N_{NO_3}$ and $\delta^{18}O_{NO_3}$) do not change during NO_3^- consumption (Casciotti et al., 2008). In contrast, NO_3^- production (e.g., nitrification) causes distinct consequences in $\delta^{15}N_{NO_3}$ and $\delta^{18}O_{NO_3}$, developing changes in Δ(15–18; Casciotti et al., 2008). The $\delta^{15}N$ of newly produced NO_3^- via nitrification mainly depends on the $\delta^{15}N$ of organic N that is remineralized, whereas the $\delta^{18}O$ of newly nitrified NO_3^- is close to the $\delta^{18}O$ of ambient water (Buchwald et al., 2012; Sigman, DiFiore, Hain, Deutsch, Wang, et al., 2009). Thus, a coupled analysis of $\delta^{15}N_{NO_3}$ and $\delta^{18}O_{NO_3}$, as well as Δ(15–18) can identify and/or distinguish nitrate production and consumption, thus improving

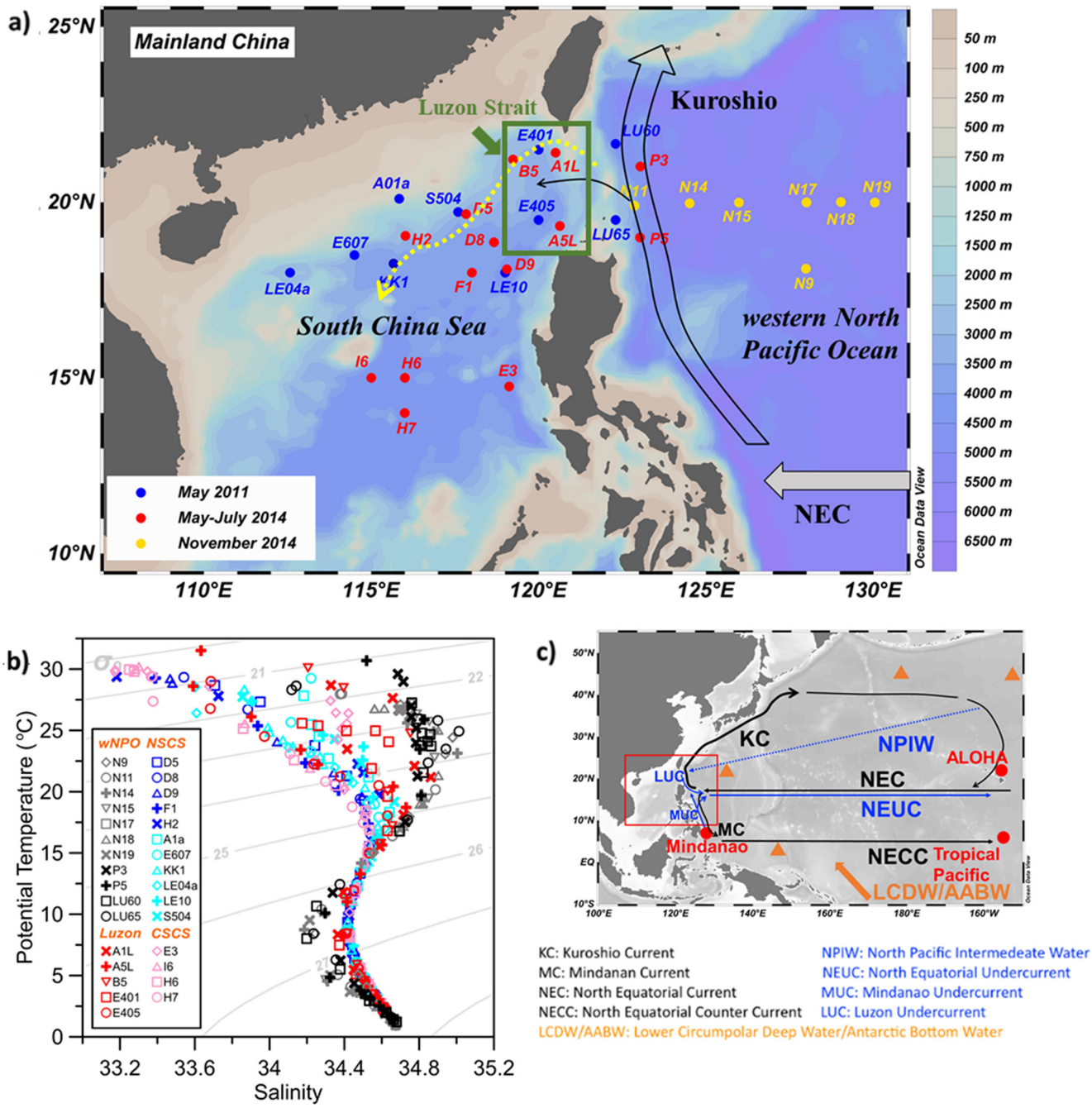

Figure 1. (a) Sampling sites in the South China Sea (SCS) and the western North Pacific Ocean (wNPO). The main routes of the Kuroshio and North Equatorial Current (NEC) are shown as black and gray broad arrows. The pathways of the Kuroshio and wNPO deep water that intrude into the SCS are presented as black solid and yellow dotted arrows, respectively (Qu et al., 2006). The sampling sites within the Luzon Strait are enclosed by a dark green box. The stations in the same cruise are marked as the same colored dots. (b) Relationship between potential temperature and salinity at stations in the wNPO (gray and black), northern (blue and cyan) and central (pink) SCS, and Luzon Strait (red). *Note.* Stations with different colors in the wNPO and northern SCS are from the different cruises shown in (a). (c) Major surface (black arrows), subsurface (blue arrows) and deep (orange arrows) currents in the Pacific (Hu et al., 2015). The path of the North Pacific Intermediate Water (NPIW) is also indicated as blue dashed line (You et al., 2005). The locations of the three sites shown in Table 2 are marked as red dots. The orange triangles denote the regions that have deep vertical mixing.

our understanding of NO_3^- dynamics in complex oceanic environments (Bourbonnais et al., 2009; Sigman et al., 2005; Wankel et al., 2007).

To date, only a limited number of studies on $\delta^{15}N_{NO_3}$ in the water column of the SCS basin and the adjacent wNPO have showed a $\delta^{15}N_{NO_3}$ minimum in the subsurface waters, which is mainly explained by an accumulation of ^{15}N-depleted signals resulting from N_2 fixation (Liu et al., 1996; Loick et al., 2007; Ren et al., 2017; Wong et al., 2002; Yang et al., 2017, 2018). However, roles of AND in lowering the subsurface $\delta^{15}N_{NO_3}$ are not well evaluated in these regions (Yang et al., 2014). On the other hand, a $\delta^{18}O_{NO_3}$ data set in the SCS basin is still lacking, which impedes understanding of NO_3^- production especially occurring in the upper water column. Furthermore, previous studies have suggested that the hydrographic features in the SCS and the wNPO are modulated by the Pacific circulation and the communication of water masses through the LS (Hu et al., 2015; Qu et al., 2006; You et al., 2005). Yet, there have been no attempts exploring how the physical processes shape nitrate isotopes in these regions.

Based on the first report of coupled analysis of $\delta^{15}N_{NO_3}$ and $\delta^{18}O_{NO_3}$ encompassing the entire water column of the SCS basin and the adjacent wNPO (Figure 1), this study aims to shed light on how biogeochemical processes and water exchange influence NO_3^- dynamics in these regions, which improves understanding of nitrogen cycling in the water column and paleoceanographic reconstruction using sedimentary archives in the Pacific Ocean and its marginal seas.

2. Materials and Methods

Field observations were conducted at 31 stations in the SCS basin and the neighboring wNPO onboard the R/V *Dongfanghong II* during May 2011, May-July 2014 and November 2014 (Figure 1a). At each site, water samples were taken at 12–30 layers for the entire water column (3,000–5,000 m) from 1 to 3 hydrocasts using a conductivity-temperature-depth (SBE 911 plus) rosette assembly equipped with 12 L Niskin bottles. Samples for nutrient measurement (n = 500) were collected in acid-cleaned polyethylene bottles and then stored at 4°C. Concentrations of nitrate plus nitrite ($[NO_3^- + NO_2^-]$), nitrite ($[NO_2^-]$), and phosphate ($[PO_4^{3-}]$) were analyzed onboard using a Technicon AA3 Auto-Analyzer (Ban-Lube, GmbH) according to Du et al. (2013). The detection limits for nitrate plus nitrite, nitrite and phosphate were 0.03 μmol kg^{-1}, 0.02 μmol kg^{-1}, 0.03 μmol kg^{-1}, respectively (Du et al., 2013). The analytical precision was better than ±1% for nitrate plus nitrite, ±1% for nitrite and ±2% for phosphate (Han et al., 2012). There were 405 samples with nutrient concentrations above the detection limits. At most sampling depths, $[NO_2^-]$ was below the detection limit, and the ratios of $[NO_2^-]$ to $[NO_3^- + NO_2^-]$ (NO_2%) were less than 1%. Only a few samples collected at the primary nitrite maximum layer (typically centered at ~75 m) had $[NO_2^-]$ of 0.21–0.45 μmol kg^{-1}, corresponding to NO_2% of 0.3–16%. Hereafter, $[NO_3^- + NO_2^-]$ is reported as $[NO_3^-]$. The nitrate anomaly (N*), a quasi-conservative tracer that indicates the deviation of water-column NO_3^-:PO_4^{3-} from the Redfield ratio (16:1), was defined as $[NO_3^-]$ minus 16 × $[PO_4^{3-}]$ (Deutsch et al., 2001). Dissolved oxygen (DO) was determined using the spectrophotometric Winkler method (Labasque et al., 2004; Pai et al., 1993). The detection limit for DO was 0.6 μmol kg^{-1} and the analytical precision was better than ±0.5%.

Samples for nitrate isotope analysis were recovered unfiltered in the high-density polyethylene bottles (Nalgene, 125 mL) that were rinsed with in situ sample water before filling and frozen at −20°C (Yang et al., 2017). For samples with $[NO_3^-]$ greater than 0.5 μmol kg^{-1} (n = 364), their $\delta^{15}N_{NO_3}$ and $\delta^{18}O_{NO_3}$ values were measured by the "denitrifier" method (Casciotti et al., 2002; Sigman et al., 2001). Briefly, 10 or 20 nmol of nitrate and nitrite were quantitatively converted to nitrous oxide (N_2O) gas using denitrifying bacteria that lack N_2O reductase. N and O isotopes of this N_2O gas were then measured on a continuous flow Gasbench II-IRMS system. Two international isotopic references (IAEA-N3 and USGS34) and a laboratory working standard (with a $\delta^{15}N_{NO_3}$ value of 13.8‰) were used to calibrate the measured $\delta^{15}N_{NO_3}$ values of samples, while three international isotopic references (IAEA-N3, USGS32, and USGS34) were applied to calibrate the $\delta^{18}O_{NO_3}$ values of samples. The standard deviations were ±0.2‰ for $\delta^{15}N_{NO_3}$ and ±0.3‰ for $\delta^{18}O_{NO_3}$ based on replicates of samples and isotopic standards (n = 3–4) in each batch of analyses; these values were consistent with our previous measurements (Yang et al., 2014). All the acronyms shown in the text are summarized in Table 1.

Table 1
Information for the Acronyms in the Text

Acronym	Full name
AABW	Antarctic Bottom Water
AND	Atmospheric nitrogen deposition
BW	Bottom water
DW	Deep water
EZ	Euphotic zone
KC	Kuroshio Current
LCDW	Lower Circumpolar Deep Water
LIW	Lower intermediate water
LS	Luzon Strait
MinIW	Mindanao Intermediate Water
NPDW	North Pacific Deep Water
NPIW	North Pacific Intermediate Water
SCS	South China Sea
SSW	Subsurface water
SW	Surface water
TPIW	Tropical Pacific Intermediate Water
TW	Thermocline water
UIW	Upper intermediate water
wNPO	western North Pacific Ocean

3. Results

3.1. Physical and Chemical Properties of Water Masses in the SCS and wNPO

Based on the observed temperature and salinity distributions at different density surfaces and literature reports (Li et al., 2002; You et al., 2005), we first classified water masses in the SCS and wNPO (Table 2): surface water (SW; potential density anomaly $\sigma_\theta < 24.0$ kg m^{-3}), subsurface water (SSW; $\sigma_\theta = 24.0$–25.0 kg m^{-3}), thermocline water (TW; $\sigma_\theta = 25.0$–26.5 kg m^{-3}), upper intermediate water (UIW; $\sigma_\theta = 26.5$–27.1 kg m^{-3}), lower intermediate water (LIW; $\sigma_\theta = 27.1$–27.6 kg m^{-3}), deep water (DW; $\sigma_\theta = 27.6$–27.7 kg m^{-3}), and bottom water (BW; $\sigma_\theta > 27.7$ kg m^{-3}). In addition, a transect passing through the wNPO, the LS, and northern and central SCS basin was examined in detail to better assess the spatial variations in the physical and chemical properties of different water masses (Figure 2).

The physical and chemical properties of these water masses in the SCS and wNPO were distinct (Figure 2 and Figure S1 in Supporting Information S1). According to the potential temperature-salinity (θ-S) diagram (Figure 1b), we found the relationship between potential temperature and salinity in both regions exhibited similar patterns. At $\sigma_\theta < 26.0$ kg m^{-3}, however, the wNPO waters were warmer and more saline than the SCS waters. A salinity maximum was observed in the wNPO SSW centered at $\sigma_\theta = \sim 24.0$ kg m^{-3} (150–200 m), whereas the SCS SSW showed a less pronounced salinity maximum. Mixing signals of waters above the thermocline between the SCS and wNPO were found at sites near the LS (in the dashed green box in Figure 1a) due to the KC intrusion. In addition, along these density surfaces, DO concentrations decreased from the wNPO to the SCS basin (Figure 2b). The SCS UIW and wNPO UIW were characterized by salinity minima centered at $\sigma_\theta = 26.5$–26.8 kg m^{-3} that were more evident in the wNPO (Figure 1b). The salinity minimum layer was uplifted by ~200 m from the wNPO to the SCS basin (Figure 2a). Oxygen minimum layers were found in both the SCS LIW and wNPO LIW at $\sigma_\theta = 27.1$–27.2 kg m^{-3}, with lower DO concentrations in the wNPO. For deep waters below 2,000 m, the θ-S distributions in the SCS basin tended to be uniform and were congruent with those in the wNPO DW at 1,500–2,500 m. Such a consistency was also reflected in the DO concentrations in these waters. The underlying wNPO BW was slightly colder, more saline, and had a higher DO concentration (Table 2).

NO_3^- distributions were also distinguishable in the SCS basin and wNPO (Figures 2c and 3a). While the SCS SW and wNPO SW were nitrate-depleted, the nitracline depth at 50 m in the SCS basin was significantly shallower than that in the wNPO (100–125 m; Figure S2 in Supporting Information S1). This suggests an extremely oligotrophic feature in wNPO SW. Below the nitracline, [NO_3^-] increased dramatically with depth from SSW toward UIW in both regions, showing higher values in the SCS basin along isopycnals (t test, $p < 0.01$). Conversely, [NO_3^-] in the underlying LIW averaged 36.8 ± 1.3 μmol kg^{-1} in the SCS basin, which was lower than that in the wNPO (39.0 ± 1.1 μmol kg^{-1}; t test, $p < 0.01$). The SCS DW and wNPO DW had comparable [NO_3^-] of ~38.6 μmol kg^{-1}. At deeper depths, [NO_3^-] in the wNPO BW decreased to ~36 μmol kg^{-1} near the bottom (Figure 3a; t test, $p < 0.01$).

The N* values in the water masses corresponding to $\sigma_\theta < 26.5$ kg m^{-3} were remarkably higher than those in the underlying water masses in the SCS basin and the wNPO, averaging between −0.4 and −2.2 μmol kg^{-1} (Table 2 and Figure 4a). In particular, the N* maximum occurred in the wNPO SSW. In the intermediate waters, N* decreased significantly to mean values of ~–6.9 μmol kg^{-1} in both regions. Below the intermediate waters, the mean N* values appeared to remain constant in the SCS but decreased slightly in the wNPO (Table 2). It is worth noting that the N* values showed spatial variations in the deep and bottom waters, with higher N* values in the open wNPO regions (sites N14–N19) compared with those at sites close to the LS and in the SCS basin (Figure 5c).

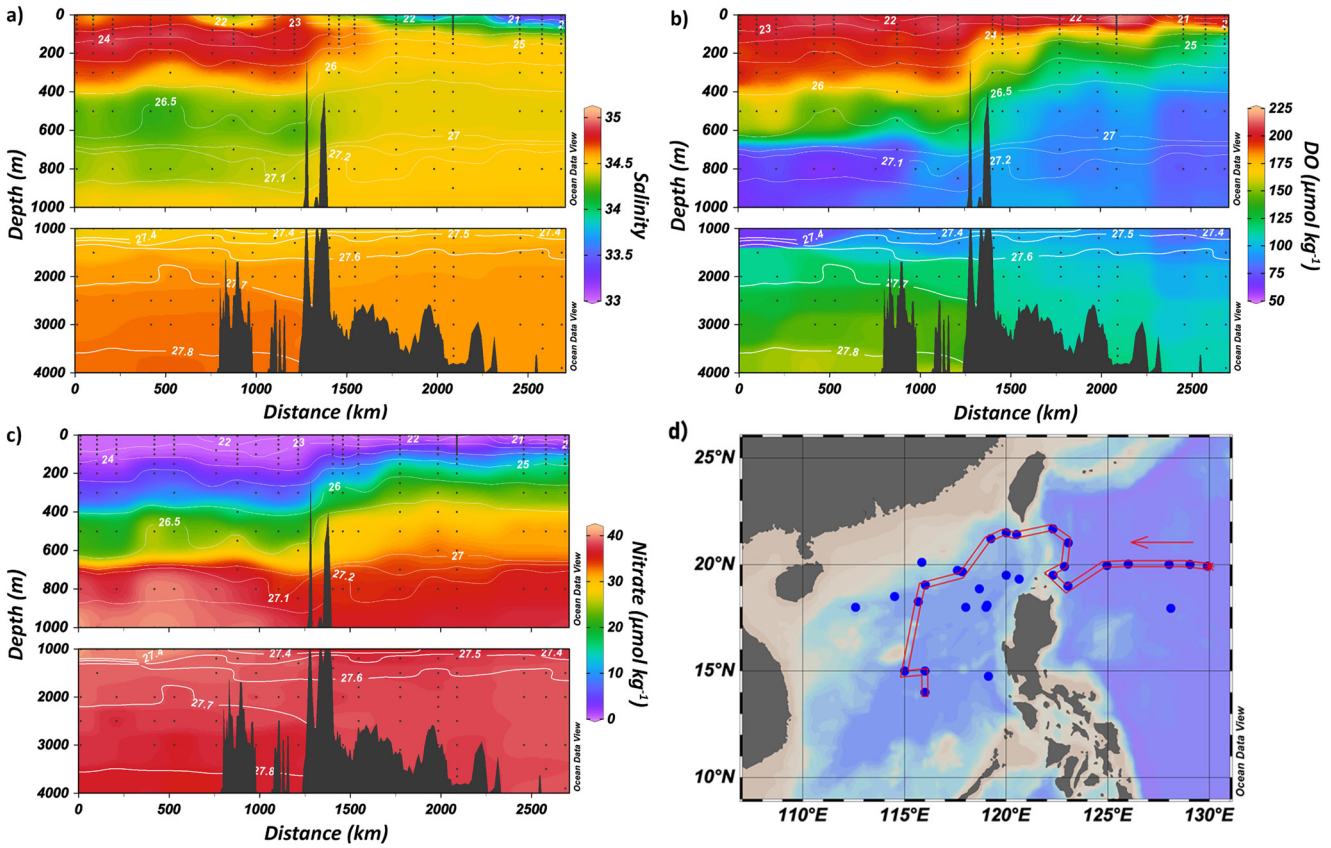

Figure 2. Distributions of salinity (a), DO (b), and nitrate (c) along the transect from the western North Pacific Ocean (wNPO) (0 km) to the central South China Sea (SCS) (d). Contours in (a–c) indicate the potential density anomaly σ_θ (kg m^{-3}).

3.2. Nitrate N and O Isotopes in the SCS and wNPO

The profiles of $\delta^{15}N_{NO_3}$ and $\delta^{18}O_{NO_3}$ were different between the SCS and wNPO, especially from intermediate to surface waters (Figure 3). Steep increases in $\delta^{15}N_{NO_3}$ and $\delta^{18}O_{NO_3}$ in the SCS SW were observed from the base of the euphotic zone (EZ) toward the surface, reaching up to ~10‰ at ~50 m (Figure 3). The corresponding Δ(15–18) decreased toward the surface (Figure 4), suggesting greater increases in $\delta^{18}O_{NO_3}$ relative to $\delta^{15}N_{NO_3}$. This feature was not detected in the wNPO SW due to the absence of nitrate in the entire EZ. Below the EZ, $\delta^{15}N_{NO_3}$ and $\delta^{18}O_{NO_3}$ minima were clearly found in both the SCS SSW and wNPO SSW. The average $\delta^{15}N_{NO_3}$ value of 2.6‰ in the wNPO SSW was ~2.1‰ lower than that in the SCS SSW, whereas its average $\delta^{18}O_{NO_3}$ value of 1.7‰ was only 0.8‰ lower than that in the SCS SSW (Table 2). Thus, the average Δ(15–18) value of 2.1 ± 0.5‰ in the SCS SSW was lower than that (0.9 ± 0.5‰) in the wNPO SSW (t test, $p < 0.01$). Nitrate N and O isotopes increased downward in parallel with increases in [NO_3^-], reaching their maxima centered at σ_θ = ~26.5–26.8 kg m^{-3} in the SCS UIW and wNPO UIW (Figures 3 and 5). The average $\delta^{15}N_{NO_3}$ value of 6.4 ± 0.4‰ and $\delta^{18}O_{NO_3}$ value of 3.1 ± 0.4‰ in the wNPO UIW were ~0.5‰ higher than those in the SCS UIW, suggesting comparable values of Δ(15–18) between the SCS UIW and wNPO UIW (3.1–3.2‰; Table 2). The distribution of nitrate isotopes in the UIW was spatially uniform in the northern SCS basin (north of 16°N) in both 2011 and 2014, whereas relatively lower values of $\delta^{15}N_{NO_3}$ and $\delta^{18}O_{NO_3}$ were observed in the central SCS basin (south of 16°N, Figures 3 and 5), particularly at the southernmost location (site H7). The $\delta^{15}N_{NO_3}$ and $\delta^{18}O_{NO_3}$ decreased moderately below the UIW in both regions, showing consistent values between SCS DW and wNPO DW (5.4–5.5‰ and 2.0–2.2‰; Table 2). Thus, the Δ(15–18) values (3.3–3.5‰) were comparable in these waters. The $\delta^{15}N_{NO_3}$ decreased slightly to 5.2‰ (t test, $p < 0.01$), and the $\delta^{18}O_{NO_3}$ (~2.0‰) remained comparable in the wNPO BW (t test, $p > 0.05$; Table 2).

Table 2
Average Values of Salinity, Nitrate, N, $\delta^{15}N_{NO_3}$ $\delta^{18}O_{NO_3}$, Δ(15–18), and Apparent Oxygen Utilization (AOU) for Different Water Masses (See Text) in the South China Sea (SCS) and the Western North Pacific Ocean (wNPO)*

Region	σ_θ (kg m^{-3})	Water masses	Salinity	NO_3^- (μmol kg^{-1})	N* (μmol kg^{-1})	$\delta^{15}N_{NO_3}$ (‰ versus air N_2)	$\delta^{18}O_{NO_3}$ (‰ versus VSMOW)	Δ(15–18) (‰)	AOU (μmol kg^{-1})
SCS	<24.0	SCS SW	34.03 ± 0.41	1.6 ± 2.6	−1.1 ± 0.5	5.8 ± 1.4	4.1 ± 2.1	1.7 ± 0.9	8.6 ± 27.8
	24.0–25.0	SCS SSW	34.54 ± 0.12	9.5 ± 3.2	−1.0 ± 0.5	4.7 ± 0.4	2.5 ± 0.7	2.1 ± 0.5	79.5 ± 26.2
	25.0–26.5	SCS TW	34.51 ± 0.07	18.0 ± 4.6	−2.2 ± 1.0	5.5 ± 0.5	2.6 ± 0.6	2.9 ± 0.4	124.7 ± 28.1
	26.5–27.1	SCS UIW	34.42 ± 0.02	30.5 ± 1.9	−4.9 ± 1.0	5.9 ± 0.3	2.8 ± 0.4	3.1 ± 0.3	193.1 ± 13.5
	27.1–27.6	SCS LIW	34.53 ± 0.04	36.8 ± 1.3	−6.7 ± 0.9	5.7 ± 0.2	2.4 ± 0.4	3.3 ± 0.2	223.3 ± 7.0
	27.6–27.7	SCS DW	34.62 ± 0.01	38.6 ± 0.4	−6.9 ± 0.8	5.5 ± 0.2	2.2 ± 0.3	3.3 ± 0.3	222.6 ± 4.6
wNPO	<24.0	wNPO SW	34.74 ± 0.18	0.2 ± 0.2	−1.0 ± 0.2	N.A.[a]	N.A.	N.A.	−0.5 ± 9.1
	24.0–25.0	wNPO SSW	34.83 ± 0.03	2.3 ± 0.8	−0.4 ± 0.6	2.6 ± 0.5	1.7 ± 0.9	0.9 ± 0.5	25.4 ± 4.4
	25.0–26.5	wNPO TW	34.51 ± 0.21	12.6 ± 7.2	−1.7 ± 1.6	5.3 ± 1.0	2.9 ± 0.4	2.4 ± 0.8	75.8 ± 37.3
	26.5–27.1	wNPO UIW	34.25 ± 0.08	29.4 ± 4.5	−5.5 ± 2.5	6.5 ± 0.4	3.3 ± 0.2	3.2 ± 0.5	176.6 ± 36.7
	27.1–27.6	wNPO LIW	34.44 ± 0.08	39.0 ± 1.1	−6.8 ± 1.3	6.0 ± 0.3	2.5 ± 0.4	3.5 ± 0.3	237.9 ± 9.5
	27.6–27.7	wNPO DW	34.61 ± 0.02	38.7 ± 0.5	−6.3 ± 1.6	5.4 ± 0.2	2.0 ± 0.3	3.5 ± 0.2	215.6 ± 3.8
	>27.7	wNPO BW	34.66 ± 0.01	37.2 ± 0.9	−5.9 ± 1.5	5.2 ± 0.2	2.0 ± 0.2	3.2 ± 0.2	195.9 ± 11.0
ALOHA[b]	26.5–27.1	$NPIW_{aloha}$	34.12 ± 0.08	33.7 ± 4.8	−5.6 ± 1.3	6.8 ± 0.3	3.4 ± 0.4	3.4 ± 0.3	221.3 ± 42.7
Tropical Pacific[c]	26.5–27.1	TPIW	34.63 ± 0.05	35.9 ± 2.2	−6.4 ± 1.0	7.7 ± 0.3	3.8 ± 0.4	3.9 ± 0.4	N.A.
Mindanao[d]	26.5–27.1	MinIW	34.38 ± 0.06	31.8 ± 3.3	−5.8 ± 0.4	7.0 ± 0.2	3.4 ± 0.3	3.6 ± 0.2	177.9 ± 12.9

Note. N.A. indicates "not available" measurements. Parameters for the intermediate waters of Station ALOHA (158°W, 23°N; $NPIW_{aloha}$) and two sites influenced by waters from the south (Mindanao at 127°E, 8°N, MinIW; Tropical Pacific at 155°W, 7°N, TPIW) are shown for comparison.

[a]N.A. indicates "not available" measurements. [b]Data obtained from Sigman, DiFiore, Hain, Deutsch, and Karl (2009). [c]Data obtained from Rafter et al. (2012, 2013). [d]Data obtained from Lehmann et al. (2018).

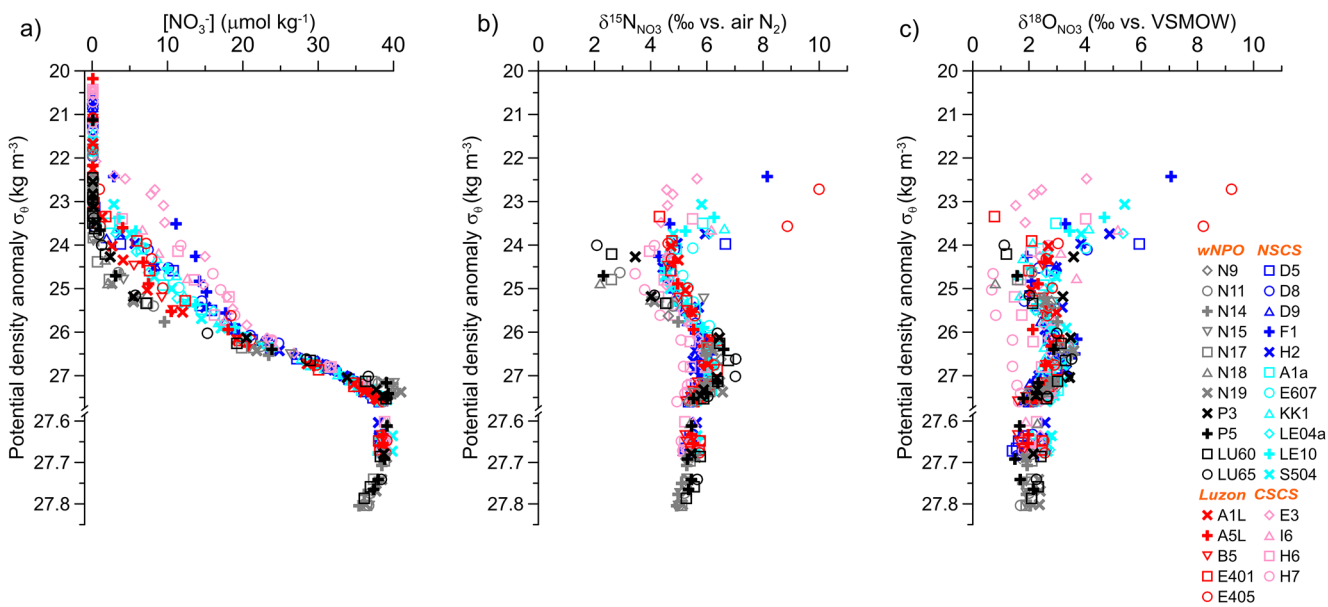

Figure 3. Isopycnal profiles of [NO_3^-] (a), $\delta^{15}N_{NO_3}$(b), and $\delta^{18}O_{NO_3}$ (c) in the northern and central South China Sea (NSCS and CSCS, respectively) and the western North Pacific Ocean (wNPO). The data from the five sites located close to the Luzon Strait (see Figure 1) are also shown.

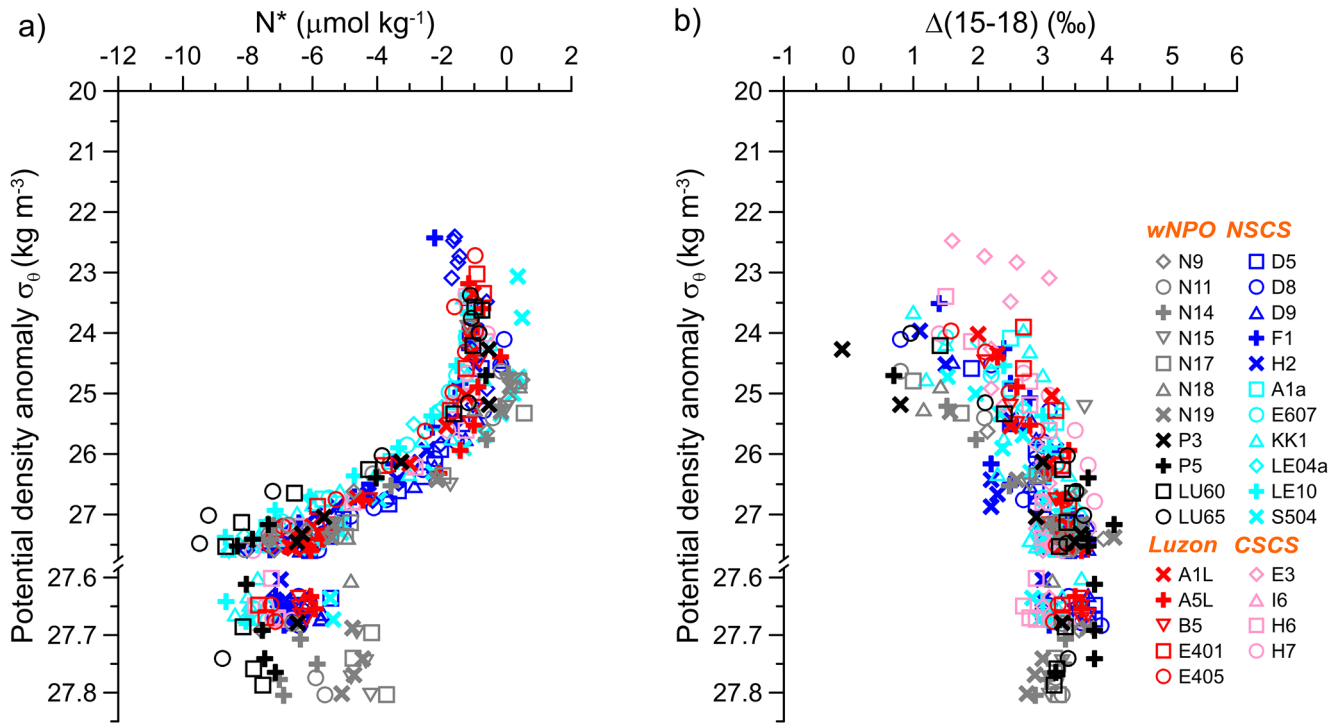

Figure 4. Same as that for Figure 3, except for the depth profiles of N* (a) and Δ(15–18) (b).

4. Discussion

4.1. Mechanisms Regulating Nitrate Isotopes in the Euphotic Zone

In contrast to an oligotrophic condition for the entire EZ in the wNPO, nitrate was clearly detectable in the lower EZ in the SCS; its concentration increased from nearly detection limits at ~50 m to 8.4 ± 3.0 μmol kg^{-1} at 100 m (Figure 2c). Such a shallow nitracline within the EZ has been observed in the SCS basin throughout the year (Du et al., 2013). Significant increases in $\delta^{15}N_{NO_3}$ and $\delta^{18}O_{NO_3}$ in the lower EZ of the SCS could thus be mainly attributed to the partial assimilation of nitrate by phytoplankton. However, greater increases in $\delta^{18}O_{NO_3}$ relative to $\delta^{15}N_{NO_3}$ suggested by a decreasing trend of Δ(15–18) within the SCS SW cannot be explained only by the partial assimilation of nitrate (e.g., Casciotti et al., 2008). The deviation of the $\delta^{15}N_{NO_3}/\delta^{18}O_{NO_3}$ ratio above the 1:1 line (with a slope of 1.3 in the linear regression relationship; $R^2 = 0.86$, $p < 0.01$, $n = 44$; Figure 6a) suggests a visible effect of the remineralization of newly formed organic N on the EZ nitrate isotope characteristics. Partial nitrate assimilation with net isotope fractionation produces ^{15}N-depleted organic N, and the decomposition of this organic N followed by nitrification lowers the ambient nitrate δ^{15}N and Δ(15–18) in seawater (Rafter et al., 2013; Wankel et al., 2007).

Nitrification in the lower portion of the EZ is likely important in oceans with a shallow nitracline, as in the SCS; its rates were as high as 25 nmol N L^{-1} day^{-1} in the lower EZ during the 2014 cruise (Wan et al., 2018). Alternatively, we assume that based on the Rayleigh model, N and O isotope effects ($^{15}\varepsilon$ and $^{18}\varepsilon$) during nitrate assimilation vary between 2‰ and 5‰, which are the typical values induced by prokaryotic and eukaryotic phytoplankton, respectively (Granger et al., 2010). Some data with lower $\delta^{15}N_{NO_3}$ and $\delta^{18}O_{NO_3}$ values than expected by the model further underline that, other than nitrate assimilation, the addition of regenerated nitrate is likely responsible for regulating changes in nitrate isotopes in the SCS EZ (Figures 6b and 6c).

Other mechanisms might, to some extent, play roles in lowering the Δ(15–18) values. The occurrence of nitrite, as well as external nitrogen inputs from AND and N_2 fixation, may introduce nitrogen oxide depleted in ^{15}N to the EZ and lower Δ(15–18) values (Casciotti, 2016; Chen et al., 2021; Yang et al., 2014). Nitrite in the SCS EZ was at a very low level during the cruises. The slope in the linear regression relationship between the observed $\delta^{15}N_{NO_3}$ and $\delta^{18}O_{NO_3}$ remained unchanged when the data obtained from the primary nitrite maximum layers were

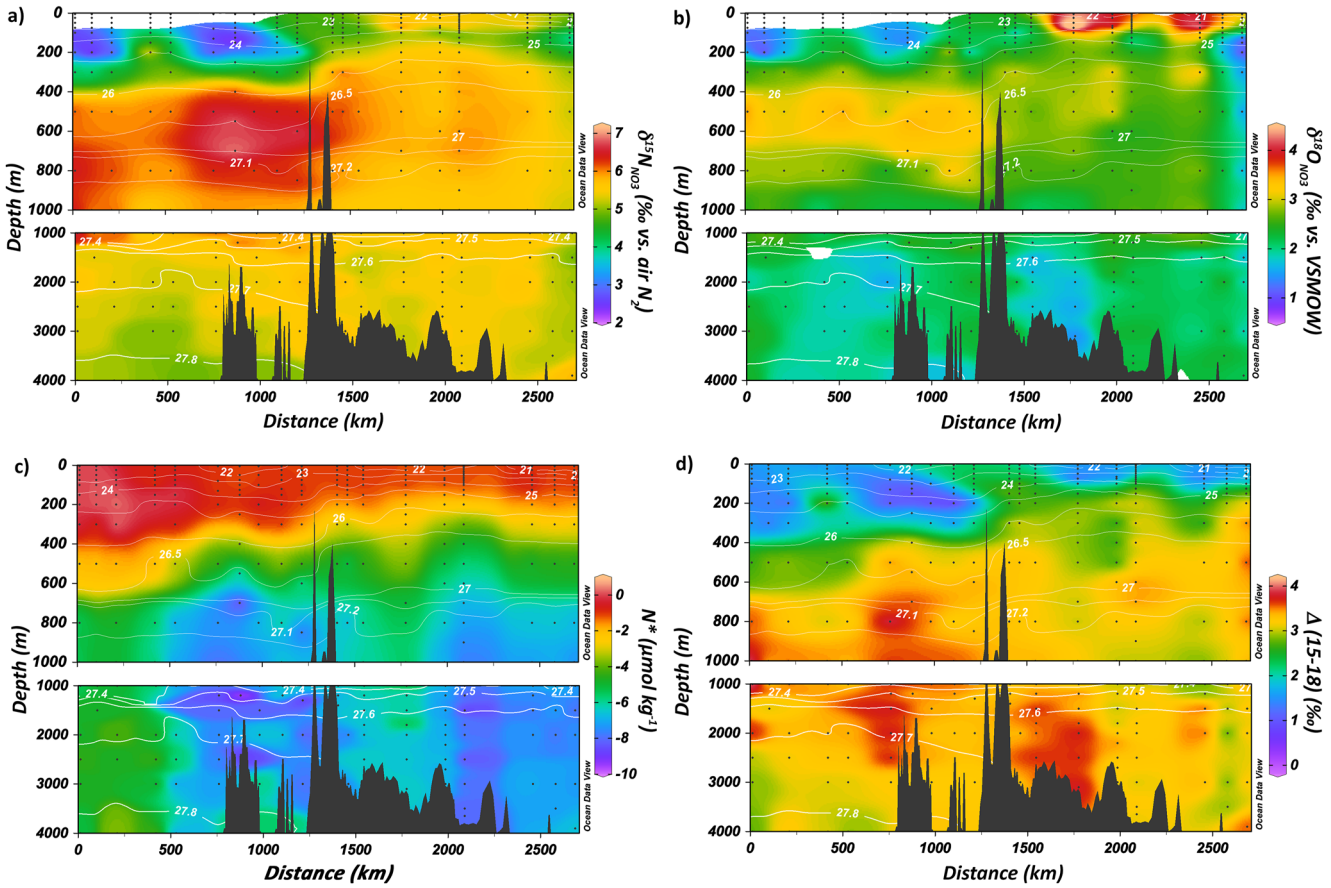

Figure 5. Distributions of $\delta^{15}N_{NO_3}$ (a), $\delta^{18}O_{NO_3}$ (b), N* (c), and Δ(15–18) (d) along the transect from the wNPO to the central SCS (the same as that in Figure 2). Contours indicate the potential density anomaly σ_θ (kg m^{-3}).

not considered. On the other hand, external N inputs that supply excess NO_3^- relative to PO_4^{3-} would induce an elevation in seawater N* (Kim et al., 2011). The lack of increases in N* toward the surface (Figure 4a), however, did not support substantial external nitrogen inputs retained in the SCS SW. In contrast, the subsurface and thermocline waters have received most external N signals, showing upward increases in N* (further discussed in

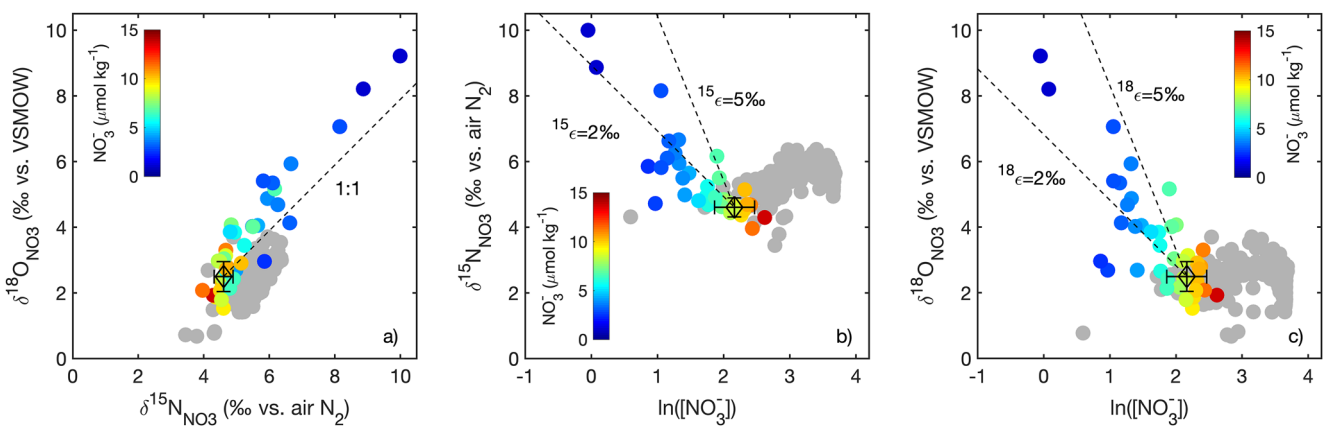

Figure 6. Plots of $\delta^{15}N_{NO_3}$ versus $\delta^{18}O_{NO_3}$ (a), $\delta^{15}N_{NO_3}$ (b) and $\delta^{18}O_{NO_3}$ (c) versus the natural logarithm of [NO_3^-] (in μmol kg^{-1}) in the South China Sea (SCS) basin. The colored and gray circles indicate the data derived from depths above and below 100 m, respectively. The open diamonds show the mean values of variables at 100 m. The dashed lines extending from the mean values in (b, c) represent the expected values of variables due to nitrate assimilation, according to the Rayleigh closed system model and isotope effects ($^{15}\varepsilon$ and $^{18}\varepsilon$) of 2‰ and 5‰.

Table 3
Estimates of the Expected Nitrate $\delta^{18}O$ in the Subsurface and Thermocline Waters of the SCS and wNPO

Water mass	$\delta^{15}N_{ext}$	$\delta^{18}O_{nit}$	$\delta^{15}N_{source}$	$\delta^{18}O_{source}$	$\delta^{15}N_{obs}$	$\delta^{18}O_{obs}$	$\delta^{18}O_{exp}$	f
SCS SSW	−2.2‰	1.1‰	5.9‰	2.8‰	4.7‰	2.5 ± 0.7‰	2.5‰	14.8%
SCS TW	−2.2‰	1.1‰	5.9‰	2.8‰	5.5‰	2.6 ± 0.6‰	2.7‰	4.9%
wNPO SSW	−1.1‰	1.1‰	6.5‰	3.3‰	2.6‰	1.7 ± 0.9‰	2.2‰	51.3%
wNPO TW	−1.1‰	1.1‰	6.5‰	3.3‰	5.3‰	2.9 ± 0.4‰	3.0‰	15.8%

Note. The related variables are discussed in Section 4.2.

Section 4.2). In addition, atmospheric nitrate generally has high ^{17}O anomaly; however, the absence of a significant ^{17}O anomaly is found in seawater NO_3^- in the SCS basin and wNPO, suggesting that atmospheric deposition has a minimal contribution to the surface NO_3^- pool (Shi et al., 2021). Therefore, we deem to have, if any, minor influences of nitrite-containing and external N inputs on the distribution of nitrate isotopes in the SCS EZ.

4.2. Signals of External Nitrate in the Subsurface and Thermocline Waters

The underlying UIW is the putative source water that eventually upwells into both the subsurface and thermocline waters (Liu & Gan, 2017). The subsurface and thermocline waters of both the SCS basin and wNPO possessed the lowest $\delta^{15}N_{NO_3}$ and the highest N* (Table 2), indicating substantial accumulation of external nitrate derived from N_2 fixation and/or AND (Bourbonnais et al., 2009; Knapp et al., 2008; Yoshikawa et al., 2015). N_2 fixation adds nitrate with $\delta^{15}N$ values between 0‰ and −2‰ (Brandes & Devol, 2002; Carpenter et al., 1997). Atmospheric nitrate is mainly new N of anthropogenic origin, and generally its annual average $\delta^{15}N$ values are negative in the study area (Shi et al., 2021; Yang et al., 2014) and other oceanic regions (Hastings et al., 2003; Kamezaki et al., 2019). In the subtropical wNPO, the mean total (dry and wet) depositional fluxes of atmospheric NO_3^- are estimated to be ∼15 μmol N m^{-2} day^{-1} or lower (Jung et al., 2011; Seok et al., 2021; Shi et al., 2021), whereas the depth-integrated rates of N_2 fixation in regions west of the LS are as high as ∼180 μmol N m^{-2} day^{-1} (Chen et al., 2014). In contrast, the observed and simulated AND fluxes in the SCS basin show identical values of ∼150 μmol N m^{-2} day^{-1}, which are higher than the N_2 fixation rates of 40–60 μmol N m^{-2} day^{-1} (Chen et al., 2014; Kim et al., 2014; Yang et al., 2014). Thus, the controlling mechanisms that lower $\delta^{15}N_{NO_3}$ and elevate N* from the UIW toward the SSW are spatially distinct, with N_2 fixation dominating in the wNPO and AND prevailing in the SCS.

Furthermore, we assess whether the accumulated signals from external nitrate can account for the observed $\delta^{18}O_{NO_3}$ and $\delta^{15}N_{NO_3}$ pattern in the subsurface and thermocline waters of the SCS and wNPO based on a two-end-member mass and isotope balance (Table 3):

$$\delta^{15}N_{obs} = \delta^{15}N_{source} \times (1 - f) + \delta^{15}N_{ext} \times f \quad (1)$$

$$\delta^{18}O_{exp} = \delta^{18}O_{source} \times (1 - f) + \delta^{18}O_{nit} \times f \quad (2)$$

where f denotes the fraction of external nitrate contributing to the nitrate isotopes of specific water masses and $\delta^{18}O_{nit}$ adopts the empirical value for ocean nitrification (1.1‰; Sigman, DiFiore, Hain, Deutsch, Wang, et al., 2009). The observed annual average nitrate $\delta^{15}N$ is −1.0‰ for N_2 fixation and −2.6‰ for AND in both regions (Yang et al., 2014). Along with the observed N_2 fixation and AND fluxes indicated above, we estimate that the flux-weighted average $\delta^{15}N$ of accumulated external nitrate ($\delta^{15}N_{ext}$) is −1.1‰ in the wNPO (N_2 fixation flux of 180 μmol N m^{-2} day^{-1} and AND flux of 15 μmol N m^{-2} day^{-1}) and −2.2‰ in the SCS basin (N_2 fixation flux of 50 μmol N m^{-2} day^{-1} and AND flux of 150 μmol N m^{-2} day^{-1}). Nitrate isotopes of source waters ($\delta^{15}N_{source}$ and $\delta^{18}O_{source}$) are identical to those of UIW in the regions. Remarkably, the expected nitrate $\delta^{18}O$ ($\delta^{18}O_{exp}$) values for the subsurface and thermocline waters of both the SCS and wNPO calculated from Equations 1 and 2, albeit with uncertainties, are in accordance with the observed $\delta^{18}O_{NO_3}$ values (Table 3). Thus, the mass and isotope balance calculations further support that decreases in $\delta^{15}N_{NO_3}$ and $\delta^{18}O_{NO_3}$ are largely attributed to the effect of external nitrate that is mostly retained in these waters. This effect is amplified in the wNPO

because lower nitrate concentrations therein may permit a comparable quantity of external nitrate inputs to induce a greater effect. Moreover, obviously lower $\delta^{15}N_{NO_3}$ and $\delta^{18}O_{NO_3}$ values observed at the southernmost site (H7) of the SCS may imply a greater accumulation of external nitrate in the central basin.

4.3. Communication of Intermediate Waters Between the SCS and wNPO

North Pacific Intermediate Water (NPIW) that forms in the subarctic Pacific spreads into the subtropical North Pacific with minimum salinity values (34.0–34.3) and eventually flows westward into the SCS (You et al., 2005). Along its isopycnal path, the production/regeneration cycle of sinking organic matter together with ocean circulation transmits the isotopically heavy nitrate of pelagic denitrification beyond the suboxic zone of the Eastern Tropical North Pacific, overprinting the original isotopic signal of NPIW (Liu et al., 1996; Sigman, DiFiore, Hain, Deutsch, & Karl, 2009). Both the wNPO UIW and SCS UIW, centered at σ_θ = 26.5–27.1 kg m^{-3} corresponding to NPIW, were characterized by a salinity minimum and the highest $\delta^{15}N_{NO_3}$ and $\delta^{18}O_{NO_3}$ values in the region (Table 2). This finding is consistent with previous studies suggesting the advection of isotopically enriched nitrate and considerably low N* from the Eastern Equatorial Pacific to the Western Equatorial Pacific (Kienast et al., 2008; Lehmann et al., 2018; Yoshikawa et al., 2006). In addition, it is evident that the signals of low N* and low DO in the intermediate waters originated from the Eastern Tropical North Pacific are transited into the wNPO UIW (Figure S3 in Supporting Information S1). These results together support that NPIW-like features are transported further into the western North Pacific and its margins, where they shape the hydrographic properties and nitrate isotopes of those intermediate waters.

We note that the hydrographic properties and nitrate isotopes of wNPO UIW differ from those of its possible isopycnal upstream in the North Pacific Subtropical Gyre (NPSG), such as the $NPIW_{aloha}$ observed at Station ALOHA (Table 2). Compared to the $NPIW_{aloha}$ (Sigman, DiFiore, Hain, Deutsch, & Karl, 2009), the wNPO UIW is relatively salty, low in [NO_3^-], and depleted in $\delta^{15}N_{NO_3}$ and $\delta^{18}O_{NO_3}$. Due to the intensive eddy-induced mixing with overlying thermocline water, NPIW becomes salty in transit from the central NPSG (e.g., Station ALOHA) to its western boundary (Yang et al., 2013). In this manner, it can be expected that this mixing may lower the [NO_3^-] and nitrate isotopic compositions of intermediate waters, as we have observed in the wNPO UIW (Figure 7 and Figure S4 in Supporting Information S1). Our data suggest that the hydrographic properties and nitrate isotopes of wNPO UIW are largely explained by the NPIW transported from the NPSG and incorporate the impact of overlying thermocline water.

One may argue that the observed seasonal outflow of SCS UIW to the wNPO (Tian et al., 2006) could modify the wNPO UIW characteristics since SCS UIW contains relatively lower $\delta^{15}N_{NO_3}$ and $\delta^{18}O_{NO_3}$ values (Table 2 and Figure 7). However, according to the distributions of radionuclide ^{226}Ra and water isotopes, this outflow is mainly blocked by the northward KC and confined to the LS (Chen, 2005; Wu et al., 2021), stretching the plausibility of this argument. In addition, tropical intermediate waters appear to be possible candidates for interpreting our data obtained in the wNPO (e.g., Tropical Pacific Intermediate Water, TPIW (Rafter et al., 2012, 2013) and Mindanao Intermediate Water, MinIW (Lehmann et al., 2018, Table 2 and Figure 7). These waters are not on the path of the North Equatorial Current and the following KC (Figure 1c), thereby impeding this possibility from highly influencing our study area. Nevertheless, the zonal distribution of nitrate isotopes along the North Equatorial Current needs to be assessed, which is important to determine how the middepth communication between the western and eastern North Pacific shapes the basin-wide nitrate characteristics.

We further realized that UIW from the wNPO, upon entering the SCS, becomes salty and lower in $\delta^{15}N_{NO_3}$ and $\delta^{18}O_{NO_3}$; this feature is primarily due to intensive mixing with the overlying SCS TW and underlying SCS LIW, which both have high salinity and isotopically light nitrate (Figures 7c and 7d). In this case, this mixing can also explain the observed changes in [NO_3^-], N* and apparent oxygen utilization (defined as the difference between the saturated DO concentration and the observed DO concentration in water) of the SCS UIW relative to wNPO UIW (Table 2 and Figure S4 in Supporting Information S1). These findings are supported by the observation that the diapycnal diffusivity in the SCS basin and the LS is two orders of magnitude higher than that in the wNPO (Tian et al., 2009). However, the relative influence of the overlying and underlying waters on the SCS UIW properties cannot be quantified based on our results. A numerical modeling study has showed that the subducted water from the upper layer with a net volume transport of ~0.5 Sv and the upwelled water from the lower layer

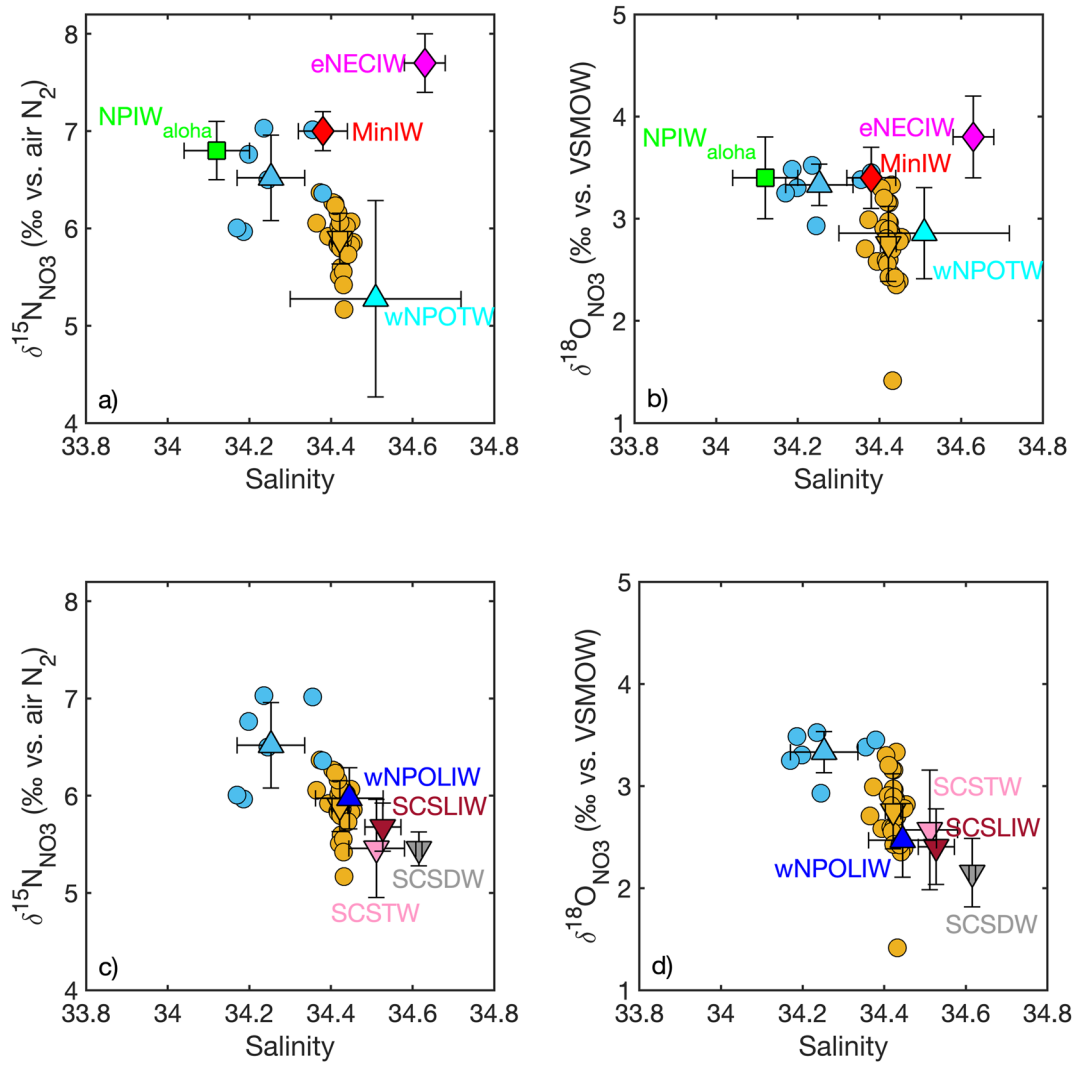

Figure 7. Comparison of salinity with nitrate N (a, c) and O (b, d) isotopes for wNPO UIW (light blue dots) and SCS UIW (orange dots). Mean values of corresponding variables are shown as upward-pointing (wNPO) and downward-pointing (SCS) triangles with the same colors. Other relevant water masses are also marked (see text). The upper and lower panels are used to discuss the wNPO UIW and SCS UIW characteristics, respectively.

with a net volume transport of ~0.9 Sv together contribute to the intermediate water in the SCS basin (Liu & Gan, 2017), which may suggest a major role of the underlying water in shaping the SCS UIW properties.

On the other hand, the hydrographic properties and nitrate isotopes of SCS LIW fit well with the result of mixing between SCS DW and SCS UIW (Figures 7c and 7d). Likewise, this mixing effect has been recorded in other geochemical tracers. For example, the seawater Nd isotopic composition ($\varepsilon Nd = (({}^{143}Nd/{}^{144}Nd_{sample})/({}^{143}Nd/{}^{144}Nd_{CHUR}) - 1) \times 10{,}000$, where CHUR stands for Chondritic Uniform Reservoir with a ${}^{143}Nd/{}^{144}Nd$ value of 0.512638) observed in the SCS LIW becomes lighter due to vertical mixing with the low-εNd SCS DW (Wu et al., 2015). Moreover, the hydrographic properties and nitrate isotopes of wNPO LIW converge to those of SCS LIW (Figures 7c and 7d and Figure S4 in Supporting Information S1), probably due to the influence of the outflow of SCS LIW (Liu & Gan, 2017). In summary, we conclude that this overflow-driven anticyclonic overturning in the SCS intermediate and deep layers largely regulates the intermediate water characteristics in the SCS and the adjoining wNPO.

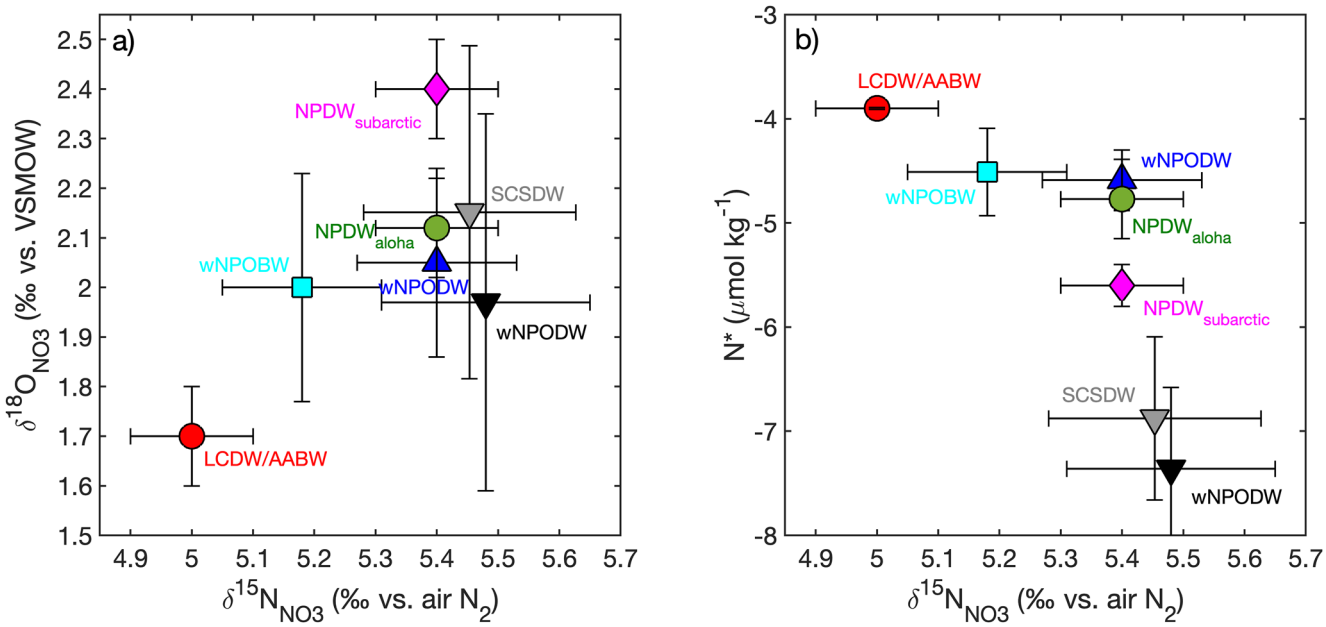

Figure 8. Plots of $\delta^{15}N_{NO_3}$ versus $\delta^{18}O_{NO_3}$ (a) and N* (b) in the deep and bottom waters of the Pacific Ocean and its margins. The relevant water masses are marked. *Note*. The wNPODW properties observed at the basin sites (blue) and at sites close to the Luzon Strait (black) are shown separately (see text). The error bars represent the standard deviation of the observed data for these water masses. The data for the $NPDW_{aloha}$, $NPDW_{subarctic}$, LCDW/AABW are compiled from Casciotti et al. (2008), Rafter et al. (2013), Sigman, DiFiore, Hain, Deutsch, and Karl (2009), Granger et al. (2011), and Yoshikawa et al. (2018) (also see Section 4.4).

4.4. Evolution of Nitrate Isotopes and N* in Deep Waters

The wNPO BW originates in the Lower Circumpolar Deep Water (LCDW) and Antarctic Bottom Water (AABW) from the south, which spreads northward to the subtropical and subarctic North Pacific bottom basin and then upwells mainly in the western and northern North Pacific to feed the North Pacific Deep Water (NPDW; Kawabe & Fujio, 2010). The LCDW and AABW moving from the South Pacific to the NPSG (e.g., Station ALOHA) have little modification in their nitrate isotopes (5.0‰ for $\delta^{15}N_{NO_3}$ and 1.7‰ for $\delta^{18}O_{NO_3}$) and N* (−3.9 μmol kg^{-1}; Casciotti et al., 2008; Rafter et al., 2013; Sigman, DiFiore, Hain, Deutsch, & Karl, 2009). In the subarctic Pacific, where the bottom water upwells and mixes with overlying water with high $\delta^{15}N_{NO_3}$ and $\delta^{18}O_{NO_3}$ and low N*, however, a slight elevation in nitrate isotopes and a modest reduction in N* are observed in the NPDW layer and deeper ($NPDW_{subarctic}$ in Figure 8; Granger et al., 2011; Yoshikawa et al., 2018). Such a combination of southern-sourced bottom water and its overlying water in the high-latitude Pacific has also been imprinted in the deep water Nd isotope signatures (Fuhr et al., 2021). As is the case in the subarctic North Pacific, the Philippine Sea close to our study area also exhibits marked upwelling in the deep layer (Kawabe & Fujio, 2010). Thus, we find that, compared with LCDW and AABW, the wNPO DW and wNPO BW at the basin sites (N9, N14–N19) have subtle but discernible increases in nitrate isotopes and decreases in N* (Figure 8a). Moreover, the NPDW properties in the NPSG ($NPDW_{aloha}$) follow the mixed signals between wNPO DW and $NPDW_{subarctic}$, with more influence by wNPO DW (Figure 8a). Compared with the subarctic Pacific deep current, the eastward deep current from the wNPO mainly contributes to the flow carrying NPDW to the NPSG interior (Kawabe & Fujio, 2010), which supports our assertion.

Notably, as the wNPO DW approaches to the oxygen-rich North Pacific margins (Figure 2b), its $\delta^{15}N_{NO_3}$ and $\delta^{18}O_{NO_3}$ remain constant (Figure 8a), while the N* is reduced by 2.5 ± 0.8 μmol kg^{-1} (Figure 8b). The most likely explanation that is currently available for this phenomenon is that increased benthic denitrification in ocean margins removes nitrate with little isotope fractionation of N and O (Lehmann et al., 2007). Given the average 1,500 m thickness of the SCS DW and its residence time of 25–40 years (Liu & Gan, 2017), the estimated average benthic denitrification rate varies between 0.26 ± 0.08 mmol N m^{-2} day^{-1} and 0.41 ± 0.13 mmol N m^{-2} day^{-1}. Although the observed benthic denitrification rate is still lacking, this estimate is comparable to the model-stimulated rates in this margin and higher than those in the Pacific basin (Bianchi et al., 2012).

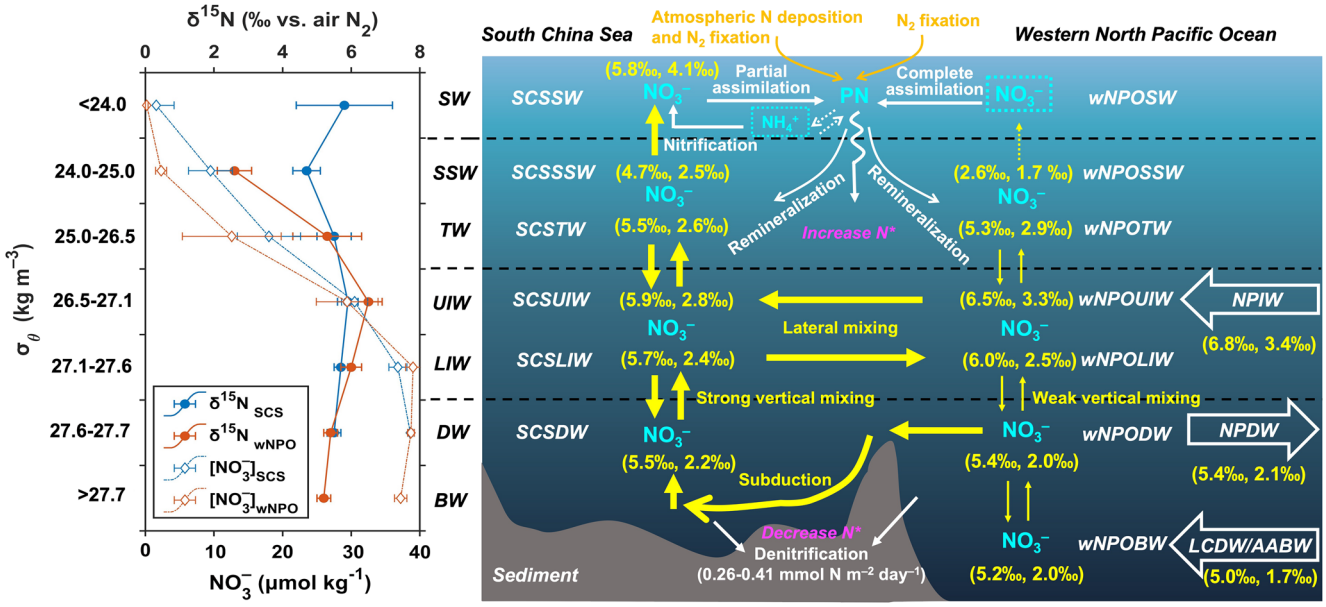

Figure 9. Conceptual diagram of biogeochemical and physical processes that determine the distribution of water-column nitrate isotopes in the SCS and wNPO. Data shown in the parentheses are nitrate N (former) and O (latter) isotopic compositions in the corresponding water mass (right panel). The left panel shows the average nitrate concentrations (diamonds) and its isotopic composition (dots) in the corresponding water masses of the SCS and wNPO (Table 2).

5. Conclusions and Implication

In this study, we elucidated the major biogeochemical and physical processes that determine the distribution of water-column nitrate isotopes in the SCS and the adjoining wNPO (Figure 9). With shallow nitracline in the SCS, disproportional increases in $\delta^{15}N_{NO_3}$ and $\delta^{18}O_{NO_3}$ can be observed in the lower EZ. This is attributed to the combined constraints of partial nitrate assimilation and EZ nitrification. Given that the nitracline in the SCS is within the EZ throughout the year, partial nitrate assimilation would produce particulate N (PN) with lower $\delta^{15}N$ relative to the upwelled nitrate. Thus, changes in nitrate utilization should be considered when using the $\delta^{15}N$ of sinking PN and sedimentary N to evaluate the relative contribution of external N to exports in the modern and past SCS. Upward decreases in $\delta^{15}N_{NO_3}$ and $\delta^{18}O_{NO_3}$ along with increasing N* in both the SCS and wNPO subsurface and thermocline waters strongly suggest a significant addition of external N that is remineralized at depth. While the amounts of external N inputs appear to be comparable in both regions, the nitrate isotopes are reduced to a lesser extent in the SCS because of the higher $[NO_3^-]$ therein.

The distribution of nitrate isotopes in the SCS intermediate and deep waters is mainly governed by lateral mixing with the wNPO waters and vertical mixing in its interior, which coincides with the influence of the observed vertical sandwich-like water flow structure through the LS (Figure 9). Clearly, the NPIW carries its isotopically enriched nitrate from the denitrification zones in the Eastern Tropical North Pacific to the wNPO and the SCS. Along this path to the wNPO, the originally high values of nitrate isotopes within the NPIW become moderate in the wNPO UIW due to mixing with overlying water that receives considerable amounts of external N. As the wNPO UIW flows into the SCS, strong vertical mixing in its interior leads to further lowering of the moderately high values of nitrate isotopes in the SCS UIW. In addition, the outflow of the underlying SCS LIW results in a zonal uniformity of nitrate isotopes in both regions. Likewise, the SCS DW retains the nitrate isotopic signals from the westward intrusive wNPO DW through the LS. However, enhanced benthic denitrification in ocean margins considerably lower N* in deep waters in and around the SCS. These findings highlight the important role of water exchange in regulating water-column N isotopes and thus sedimentary N isotope records in the SCS.

Data Availability Statement

All data used in this study are available at PANGAEA (https://doi.pangaea.de/10.1594/PANGAEA.940587; Yang, 2022).

Acknowledgments
This study was supported by the Strategic Priority Research Program of Chinese Academy of Sciences (Grant #XDB42000000), the National Natural Science Foundation of China (Grants #41890804, #41721005, #92058204), the Fundamental Research Funds for the Central Universities (Grants #20720190092, #20720212005), and the State Key Laboratory of Marine Resource Utilization in South China Sea (Hainan University; Grant #MRUKF2021018). We thank Wenbin Zou, Li Tian, Tao Huang, and Lifang Wang for the on-deck nutrient measurements and Liguo Guo for the DO measurements. We also thank three anonymous reviewers and the Editor for their constructive comments.

References

Bianchi, D., Dunne, J. P., Sarmiento, J. L., & Galbraith, E. D. (2012). Data-based estimates of suboxia, denitrification, and N_2O production in the ocean and their sensitivities to dissolved O_2. *Global Biogeochemical Cycles*, *26*, GB2009. https://doi.org/10.1029/2011GB004209

Bourbonnais, A., Lehmann, M. F., Waniek, J. J., & Schulz-Bull, D. E. (2009). Nitrate isotope anomalies reflect N_2 fixation in the Azores Front region (subtropical NE Atlantic). *Journal of Geophysical Research: Oceans*, *114*, C03003. https://doi.org/10.1029/2007JC004617

Brandes, J. A., & Devol, A. H. (2002). A global marine-fixed nitrogen isotopic budget: Implications for Holocene nitrogen cycling. *Global Biogeochemical Cycles*, *16*(4), 1120–1121. https://doi.org/10.1029/2001GB001856

Buchwald, C., Santoro, A. E., McIlvin, M. R., & Casciotti, K. L. (2012). Oxygen isotopic composition of nitrate and nitrite produced by nitrifying cocultures and natural marine assemblages. *Limnology & Oceanography*, *57*(5), 1361–1375. https://doi.org/10.4319/lo.2012.57.5.1361

Cai, Z., Gan, J., Liu, Z., Hui, C. R., & Li, J. (2020). Progress on the formation dynamics of the layered circulation in the South China Sea, *Progress in Oceanography*, *181*, 102246. https://doi.org/10.1016/j.pocean.2019.102246

Canfield, D. E., Glazer, A. N., & Falkowski, P. G. (2010). The evolution and future of Earth's nitrogen cycle. *Science*, *330*(6001), 192–196. https://doi.org/10.1126/science.1186120

Carpenter, E. J., Harvey, H. R., Fry, B., & Capone, D. G. (1997). Biogeochemical tracers of the marine cyanobacterium *Trichodesmium*. *Deep-Sea Research Part I: Oceanographic Research Papers*, *44*(1), 27–38. https://doi.org/10.1016/S0967-0637(96)00091-X

Casciotti, K. L. (2016). Nitrogen and oxygen isotopic studies of the marine nitrogen cycle. *Annual Review of Marine Science*, *8*(1), 379–407. https://doi.org/10.1146/annurev-marine-010213-135052

Casciotti, K. L., Sigman, D. M., Hastings, M. G., Bohlke, J. K., & Hilkert, A. (2002). Measurement of the oxygen isotopic composition of nitrate in seawater and freshwater using the denitrifier method. *Analytical Chemistry*, *74*(19), 4905–4912. https://doi.org/10.1021/ac020113w

Casciotti, K. L., Trull, T. W., Glover, D. M., & Davies, D. (2008). Constraints on nitrogen cycling at the subtropical North Pacific Station ALOHA from isotopic measurements of nitrate and particulate nitrogen. *Deep-Sea Research Part II: Topical Studies in Oceanography*, *55*(14–15), 1661–1672. https://doi.org/10.1016/j.dsr2.2008.04.017

Chen, C.-T. A. (2005). Tracing tropical and intermediate waters from the south China sea to the Okinawa trough and beyond. *Journal of Geophysical Research: Oceans*, *110*, C05012. https://doi.org/10.1029/2004JC002494

Chen, C.-T. A. (2010). Cross-boundary exchanges of carbon and nitrogen in continental margins. In K.-K.Liu, L.Atkinson, R.Quiñones, & L.Talaue-McManus (Eds.), *Carbon and nutrient fluxes in continental margins: A global synthesis* (pp. 561–574). Springer. https://doi.org/10.1007/978-3-540-92735-8_13

Chen, Y., Bardhan, P., Zhao, X., Zheng, M., Qiu, Y., & Chen, M. (2021). Nitrite cycle indicated by dual isotopes in the northern south China sea. *Journal of Geophysical Research: Biogeosciences*, *126*, e2020JG006129. https://doi.org/10.1029/2020JG006129

Chen, Y. L. L., Chen, H. Y., Lin, Y. H., Yong, T. C., Taniuchi, Y., & Tuo, S. H. (2014). The relative contributions of unicellular and filamentous diazotrophs to N_2 fixation in the South China Sea and the upstream Kuroshio. *Deep-Sea Research Part I: Oceanographic Research Papers*, *85*, 56–71. https://doi.org/10.1016/j.dsr.2013.11.006

Dai, M., Cao, Z., Guo, X., Zhai, W., Liu, Z., Yin, Z., et al. (2013). Why are some marginal seas sources of atmospheric CO_2? *Geophysical Research Letters*, *40*, 2154–2158. https://doi.org/10.1002/grl.50390

Deutsch, C., Gruber, N., Key, R. M., Sarmiento, J. L., & Ganachaud, A. (2001). Denitrification and N_2 fixation in the Pacific ocean. *Global Biogeochemical Cycles*, *15*(2), 483–506. https://doi.org/10.1029/2000GB001291

Doney, S. C. (2010). The growing human footprint on coastal and open-ocean biogeochemistry. *Science*, *328*(5985), 1512–1516. https://doi.org/10.1126/science.1185198

Du, C., Liu, Z., Dai, M., Kao, S. J., Cao, Z., Zhang, Y., et al. (2013). Impact of the Kuroshio intrusion on the nutrient inventory in the upper northern south China sea: Insights from an isopycnal mixing model. *Biogeosciences*, *10*, 6419–6432. https://doi.org/10.5194/bg-10-6419-2013

Emeis, K. C., Mara, P., Schlarbaum, T., Mobius, J., Dähnke, K., Struck, U., et al. (2010). External N inputs and internal N cycling traced by isotope ratios of nitrate, dissolved reduced nitrogen, and particulate nitrogen in the eastern Mediterranean Sea. *Journal of Geophysical Research: Biogeosciences*, *115*, G04041. https://doi.org/10.1029/2009JG001214

Fuhr, M., Laukert, G., Yu, Y., Nürnberg, D., & Frank, M. (2021). Tracing water mass mixing from the equatorial to the north Pacific ocean with dissolved Neodymium isotopes and concentrations. *Frontiers in Marine Science*, *7*(1261), 603761. https://doi.org/10.3389/fmars.2020.603761

Granger, J., Prokopenko, M. G., Sigman, D. M., Mordy, C. W., Morse, Z. M., Morales, L. V., et al. (2011). Coupled nitrification-denitrification in sediment of the eastern Bering Sea shelf leads to ^{15}N enrichment of fixed N in shelf waters. *Journal of Geophysical Research: Oceans*, *116*, C11006. https://doi.org/10.1029/2010JC006751

Granger, J., Sigman, D. M., Lehmann, M. F., & Tortell, P. D. (2008). Nitrogen and oxygen isotope fractionation during dissimilatory nitrate reduction by denitrifying bacteria. *Limnology & Oceanography*, *53*(6), 2533–2545. https://doi.org/10.4319/lo.2008.53.6.2533

Granger, J., Sigman, D. M., Rohde, M. M., Maldonado, M. T., & Tortell, P. D. (2010). N and O isotope effects during nitrate assimilation by unicellular prokaryotic and eukaryotic plankton cultures. *Geochimica et Cosmochimica Acta*, *74*(3), 1030–1040. https://doi.org/10.1016/j.gca.2009.10.044

Gruber, N., & Galloway, J. N. (2008). An earth-system perspective of the global nitrogen cycle. *Nature*, *451*, 293–296. https://doi.org/10.1038/nature06592

Han, A., Dai, M. H., Kao, S. J., Gan, J., Li, Q., Wang, L. F., et al. (2012). Nutrient dynamics and biological consumption in a large continental shelf system under the influence of both a river plume and coastal upwelling. *Limnology & Oceanography*, *57*(2), 486–502. https://doi.org/10.4319/lo.2012.57.2.0486

Hastings, M. G., Sigman, D. M., & Lipschultz, F. (2003). Isotopic evidence for source changes of nitrate in rain at Bermuda. *Journal of Geophysical Research: Atmospheres*, *108*(D24), 4790. https://doi.org/10.1029/2003JD003789

Higginson, M. J., Maxwell, J. R., & Altabet, M. A. (2003). Nitrogen isotope and chlorin paleoproductivity records from the northern south China sea: Remote vs. local forcing of millennial- and orbital-scale variability. *Marine Geology*, *201*(1–3), 223–250. https://doi.org/10.1016/S0025-3227(03)00218-4

Hu, D., Wu, L., Cai, W., Gupta, A. S., Ganachaud, A., Qiu, B., et al. (2015). Pacific Western boundary currents and their roles in climate. *Nature*, *522*(7556), 299–308. https://doi.org/10.1038/nature14504

Jickells, T. D., Buitenhuis, E., Altieri, K., Baker, A. R., Capone, D., Duce, R. A., et al. (2017). A reevaluation of the magnitude and impacts of anthropogenic atmospheric nitrogen inputs on the ocean. *Global Biogeochemical Cycles*, *31*, 289–305. https://doi.org/10.1002/2016GB005586

Jung, J., Furutani, H., & Uematsu, M. (2011). Atmospheric inorganic nitrogen in marine aerosol and precipitation and its deposition to the North and South Pacific Oceans. *Journal of Atmospheric Chemistry*, *68*(2), 157–181. https://doi.org/10.1007/s10874-012-9218-5

Kamezaki, K., Hattori, S., Iwamoto, Y., Ishino, S., Furutani, H., Miki, Y., et al. (2019). Tracing the sources and formation pathways of atmospheric particulate nitrate over the Pacific Ocean using stable isotopes. *Atmospheric Environment*, *209*, 152–166. https://doi.org/10.1016/j.atmosenv.2019.04.026

Kawabe, M., & Fujio, S. (2010). Pacific ocean circulation based on observation. *Journal of Oceanography*, *66*(3), 389–403. https://doi.org/10.1007/s10872-010-0034-8

Kienast, M. (2000). Unchanged nitrogen isotopic composition of organic matter in the South China Sea during the last climatic cycle: Global implications. *Paleoceanography*, *15*(2), 244–253. https://doi.org/10.1029/1999PA000407

Kienast, M., Lehmann, M. F., Timmermann, A., Galbraith, E., Bolliet, T., Holboum, A., et al. (2008). A mid-Holocene transition in the nitrogen dynamics of the Western equatorial Pacific: Evidence of a deepening thermocline? *Geophysical Research Letters*, *35*, L23610. https://doi.org/10.1029/2008GL035464

Kim, H., Lee, K., Lim, D.-I., Nam, S.-I., Kim, T.-W., Yang, J.-Y. T., et al. (2017). Widespread anthropogenic nitrogen in northwestern Pacific ocean sediment. *Environmental Science & Technology*, *51*(11), 6044–6052. https://doi.org/10.1021/acs.est.6b05316

Kim, T. W., Lee, K., Duce, R., & Liss, P. (2014). Impact of atmospheric nitrogen deposition on phytoplankton productivity in the South China Sea. *Geophysical Research Letters*, *41*, 3156–3162. https://doi.org/10.1002/2014GL059665

Kim, T. W., Lee, K., Najjar, R. G., Jeong, H. D., & Jeon, H. J. (2011). Increasing N abundance in the northwestern Pacific Ocean due to atmospheric nitrogen deposition. *Science*, *334*, 505–509. https://doi.org/10.1126/science.1206583

Knapp, A. N., DiFiore, P. J., Deutsch, C., Sigman, D. M., & Lipschultz, F. (2008). Nitrate isotopic composition between Bermuda and Puerto Rico: Implications for N_2 fixation in the Atlantic ocean. *Global Biogeochemical Cycles*, *22*, GB3014. https://doi.org/10.1029/2007GB003107

Kritee, K., Sigman, D. M., Granger, J., Ward, B. B., Jayakumar, A., & Deutsch, C. (2012). Reduced isotope fractionation by denitrification under conditions relevant to the ocean. *Geochimica et Cosmochimica Acta*, *92*, 243–259. https://doi.org/10.1016/j.gca.2012.05.020

Labasque, T., Chaumery, C., Aminot, A., & Kergoat, G. (2004). Spectrophotometric Winkler determination of dissolved oxygen: Re-examination of critical factors and reliability. *Marine Chemistry*, *88*(1–2), 53–60. https://doi.org/10.1016/j.marchem.2004.03.004

Lehmann, N., Granger, J., Kienast, M., Brown, K. S., Rafter, P. A., Martínez-Méndez, G., & Mohtadi, M. (2018). Isotopic evidence for the evolution of subsurface nitrate in the Western equatorial Pacific. *Journal of Geophysical Research: Oceans*, *123*, 1684–1707. https://doi.org/10.1002/2017JC013527

Lehmann, M. F., Sigman, D. M., McCorkle, D. C., Granger, J., Hoffmann, S., Cane, G., & Brunelle, B. G. (2007). The distribution of nitrate 15N/14N in marine sediments and the impact of benthic nitrogen loss on the isotopic composition of oceanic nitrate. *Geochimica et Cosmochimica Acta*, *71*(22), 5384–5404. https://doi.org/10.1016/j.gca.2007.07.025

Li, F., Li, L., Wang, X., & Liu, C. (2002). Water masses in the south China Sea and water exchange between the Pacific and the south China sea. *Journal of Ocean University of Qingdao*, *1*(1), 19–24. https://doi.org/10.1007/s11802-002-0025-5

Liu, K.-K., Su, M.-J., Hsueh, C.-R., & Gong, G.-C. (1996). The nitrogen isotopic composition of nitrate in the Kuroshio water northeast of Taiwan: Evidence for nitrogen fixation as a source of isotopically light nitrate. *Marine Chemistry*, *54*(3–4), 273–292. https://doi.org/10.1016/0304-4203(96)00034-5

Liu, Z., & Gan, J. (2017). Three-dimensional pathways of water masses in the south China sea: A modeling study. *Journal of Geophysical Research: Oceans*, *122*, 6039–6054. https://doi.org/10.1002/2016JC012511

Loick, N., Dippner, J., Doan, H. N., Liskow, I., & Voss, M. (2007). Pelagic nitrogen dynamics in the Vietnamese upwelling area according to stable nitrogen and carbon isotope data. *Deep-Sea Research Part I: Oceanographic Research Papers*, *54*(4), 596–607. https://doi.org/10.1016/j.dsr.2006.12.009

Marconi, D., Alexandra Weigand, M., Rafter, P. A., McIlvin, M. R., Forbes, M., Casciotti, K. L., & Sigman, D. M. (2015). Nitrate isotope distributions on the US GEOTRACES North Atlantic cross-basin section: Signals of polar nitrate sources and low latitude nitrogen cycling. *Marine Chemistry*, *177*, 143–156. https://doi.org/10.1016/j.marchem.2015.06.007

Marconi, D., Sigman, D. M., Casciotti, K. L., Campbell, E. C., Weigand, M. A., Fawcett, S. E., et al. (2017). Tropical dominance of N_2 fixation in the north Atlantic ocean. *Global Biogeochemical Cycles*, *31*, 1608–1623. https://doi.org/10.1002/2016GB005613

Moon, J.-Y., Lee, K., Lim, W.-A., Lee, E., Dai, M., Choi, Y.-H., et al. (2021). Anthropogenic nitrogen is changing the East China and Yellow seas from being N deficient to being P deficient. *Limnology & Oceanography*, *66*(3), 914–924. https://doi.org/10.1002/lno.11651

Pai, S. C., Gong, G. C., & Liu, K. K. (1993). Determination of dissolved oxygen in seawater by direct spectrophotometry of total iodine. *Marine Chemistry*, *41*(4), 343–351. https://doi.org/10.1016/0304-4203(93)90266-Q

Qu, T., Girton, J. B., & Whitehead, J. A. (2006). Deepwater overflow through Luzon Strait. *Journal of Geophysical Research: Oceans*, *111*, C01002. https://doi.org/10.1029/2005JC003139

Rafter, P. A., DiFiore, P. J., & Sigman, D. M. (2013). Coupled nitrate nitrogen and oxygen isotopes and organic matter remineralization in the Southern and Pacific Oceans. *Journal of Geophysical Research: Oceans*, *118*, 4781–4794. https://doi.org/10.1002/jgrc.20316

Rafter, P. A., Sigman, D. M., Charles, C. D., Kaiser, J., & Haug, G. H. (2012), Subsurface tropical Pacific nitrogen isotopic composition of nitrate: Biogeochemical signals and their transport, *Global Biogeochemical Cycles*, *26*, GB1003. https://doi.org/10.1029/2010GB003979

Ren, H., Sigman, D. M., Chen, M. T., & Kao, S. J. (2012). Elevated foraminifera-bound nitrogen isotopic composition during the last ice age in the South China Sea and its global and regional implications. *Global Biogeochemical Cycles*, *26*, GB1031. https://doi.org/10.1029/2010GB004020

Ren, H., Sigman, D. M., Martínez-García, A., Anderson, R. F., Chen, M.-T., Ravelo, A. C., et al. (2017). Impact of glacial/interglacial sea level change on the ocean nitrogen cycle. *Proceedings of the National Academy of Sciences of the United States of America*, *114*(33), E6759–E6766. https://doi.org/10.1073/pnas.1701315114

Seok, M.-W., Kim, D., Park, G. H., Lee, K., Kim, T. H., Jung, J., et al. (2021). Atmospheric deposition of inorganic nutrients to the Western North Pacific Ocean. *The Science of the Total Environment*, *793*, 148401. https://doi.org/10.1016/j.scitotenv.2021.148401

Shi, G., Ma, H., Zhu, Z., Hu, Z., Chen, Z., Jiang, S., et al. (2021). Using stable isotopes to distinguish atmospheric nitrate production and its contribution to the surface ocean across hemispheres. *Earth and Planetary Science Letters*, *564*, 116914. https://doi.org/10.1016/j.epsl.2021.116914

Shiozaki, T., Furuya, K., Kodama, T., Kitajima, S., Takeda, S., Takemura, T., & Kanda, J. (2010). New estimation of N_2 fixation in the Western and central Pacific Ocean and its marginal seas. *Global Biogeochemical Cycles*, *24*, GB1015. https://doi.org/10.1029/2009GB003620

Sigman, D. M., Casciotti, K. L., Andreani, M., Barford, C., Galanter, M., & Bohlke, J. K. (2001). A bacterial method for the nitrogen isotopic analysis of nitrate in seawater and freshwater. *Analytical Chemistry*, *73*(17), 4145–4153. https://doi.org/10.1021/ac010088e

Sigman, D. M., DiFiore, P. J., Hain, M. P., Deutsch, C., & Karl, D. M. (2009). Sinking organic matter spreads the nitrogen isotope signal of pelagic denitrification in the North Pacific. *Geophysical Research Letters*, *36*, L08605. https://doi.org/10.1029/2008GL035784

Sigman, D. M., DiFiore, P. J., Hain, M. P., Deutsch, C., Wang, Y., Karl, D. M., et al. (2009). The dual isotopes of deep nitrate as a constraint on the cycle and budget of oceanic fixed nitrogen. *Deep-Sea Research Part I: Oceanographic Research Papers*, *56*(9), 1419–1439. https://doi.org/10.1016/j.dsr.2009.04.007

Sigman, D. M., Granger, J., DiFiore, P. J., Lehmann, M. M., Ho, R., Cane, G., & van Geen, A. (2005). Coupled nitrogen and oxygen isotope measurements of nitrate along the eastern North Pacific margin. *Global Biogeochemical Cycles*, *19*, GB4022. https://doi.org/10.1029/2005GB002458

Tian, J., Yang, Q., Liang, X., Xie, L., Hu, D., Wang, F., & Qu, T. (2006). Observation of Luzon Strait transport. *Geophysical Research Letters*, *33*, L19607. https://doi.org/10.1029/2006GL026272

Tian, J., Yang, Q., & Zhao, W. (2009). Enhanced diapycnal mixing in the south China sea. *Journal of Physical Oceanography*, *39*(12), 3191–3203. https://doi.org/10.1175/2009jpo3899.1

Tuerena, R. E., Ganeshram, R. S., Geibert, W., Fallick, A. E., Dougans, J., Tait, A., et al. (2015). Nutrient cycling in the Atlantic basin: The evolution of nitrate isotope signatures in water masses. *Global Biogeochemical Cycles*, *29*, 1830–1844. https://doi.org/10.1002/2015GB005164

Voss, M., Bange, H. W., Dippner, J. W., Middelburg, J. J., Montoya, J. P., & Ward, B. (2013). The marine nitrogen cycle: Recent discoveries, uncertainties and the potential relevance of climate change. *Philosophical Transactions of the Royal Society B: Biological Sciences*, *368*(1621), 20130121. https://doi.org/10.1098/rstb.2013.0121

Voss, M., Dippner, J. W., & Montoya, J. P. (2001). Nitrogen isotope patterns in the oxygen-deficient waters of the eastern tropical North Pacific ocean. *Deep-Sea Research Part I: Oceanographic Research Papers*, *48*(8), 1905–1921. https://doi.org/10.1016/S0967-0637(00)00110-2

Wan, X. S., Sheng, H.-X., Dai, M., Zhang, Y., Shi, D., Trull, T. W., et al. (2018). Ambient nitrate switches the ammonium consumption pathway in the euphotic ocean. *Nature Communications*, *9*(1), 915. https://doi.org/10.1038/s41467-018-03363-0

Wankel, S. D., Kendall, C., Pennington, J. T., Chavez, F. P., & Paytan, A. (2007). Nitrification in the euphotic zone as evidenced by nitrate dual isotopic composition: Observations from Monterey Bay, California. *Global Biogeochemical Cycles*, *21*, GB2009. https://doi.org/10.1029/2006GB002723

Wong, G. T. F., Chung, S. W., Shiah, F. K., Chen, C. C., Wen, L. S., & Liu, K. K. (2002). Nitrate anomaly in the upper nutricline in the northern South China Sea—Evidence for nitrogen fixation. *Geophysical Research Letters*, *29*(23), 2097. https://doi.org/10.1029/2002GL015796

Wu, J., Lao, Q., Chen, F., Huang, C., Zhang, S., Wang, C., et al. (2021). Water mass processes between the south China Sea and the Western Pacific through the Luzon Strait: Insights from hydrogen and oxygen isotopes. *Journal of Geophysical Research: Oceans*, *126*, e2021JC017484. https://doi.org/10.1029/2021JC017484

Wu, Q., Colin, C., Liu, Z., Douville, E., Dubois-Dauphin, Q., & Frank, N. (2015). New insights into hydrological exchange between the South China Sea and the Western Pacific Ocean based on the Nd isotopic composition of seawater. *Deep-Sea Research Part II: Topical Studies in Oceanography*, *122*, 25–40. https://doi.org/10.1016/j.dsr2.2015.11.005

Xu, M. N., Zhang, W., Zhu, Y., Liu, L., Zheng, Z., Wan, X. S., et al. (2018). Enhanced ammonia oxidation caused by lateral Kuroshio intrusion in the boundary zone of the northern south China sea. *Geophysical Research Letters*, *45*, 6585–6593. https://doi.org/10.1029/2018GL077896

Yang, G., Wang, F., Li, Y., & Lin, P. (2013). Mesoscale eddies in the northwestern subtropical Pacific Ocean: Statistical characteristics and three-dimensional structures. *Journal of Geophysical Research: Oceans*, *118*, 1906–1925. https://doi.org/10.1002/jgrc.20164

Yang, J. Y. T. (2022). Nitrate isotopes in the south China Sea and the adjoining Western north Pacifc ocean. *PANGAEA*. https://doi.org/10.1594/PANGAEA.940587

Yang, J. Y. T., Hsu, S. C., Dai, M. H., Hsiao, S. S. Y., & Kao, S. J. (2014). Isotopic composition of water-soluble nitrate in bulk atmospheric deposition at Dongsha Island: Sources and implications of external N supply to the northern south China sea. *Biogeosciences*, *11*, 1833–1846. https://doi.org/10.5194/bg-11-1833-2014

Yang, J. Y. T., Kao, S. J., Dai, M., Yan, X., & Lin, H. L. (2017). Examining N cycling in the northern South China Sea from N isotopic signals in nitrate and particulate phases. *Journal of Geophysical Research: Biogeosciences*, *122*, 2118–2136. https://doi.org/10.1002/2016JG003618

Yang, Z., Chen, J., Chen, M., Ran, L., Li, H., Lin, P., et al. (2018). Sources and transformations of nitrogen in the south China sea: Insights from nitrogen isotopes. *Journal of Oceanography*, *74*(1), 101–113. https://doi.org/10.1007/s10872-017-0443-z

Yoshikawa, C., Makabe, A., Matsui, Y., Nunoura, T., & Ohkouchi, N. (2018). Nitrate isotopie distribution in the subarctic and subtropical North Pacific. *Geochemistry, Geophysics, Geosystems*, *19*, 2212–2224. https://doi.org/10.1029/2018GC007528

Yoshikawa, C., Makabe, A., Shiozaki, T., Toyoda, S., Yoshida, O., Furuya, K., & Yoshida, N. (2015). Nitrogen isotope ratios of nitrate and N* anomalies in the subtropical South Pacific. *Geochemistry, Geophysics, Geosystems*, *16*, 1439–1448. https://doi.org/10.1002/2014GC005678

Yoshikawa, C., Yamanaka, Y., & Nakatsuka, T. (2006). Nitrate-nitrogen isotopic patterns in surface waters of the Western and central equatorial Pacific. *Journal of Oceanography*, *62*, 511–525. https://doi.org/10.1007/s10872-006-0072-4

You, Y., Chern, C. S., Yang, Y., Liu, C. T., Liu, K. K., & Pai, S. C. (2005). The South China sea, a *cul-de-sac* of North Pacific intermediate water. *Journal of Oceanography*, *61*, 509–527. https://doi.org/10.1007/s10872-005-0059-6